

UC Irvine

UC Irvine Previously Published Works

Title

Wintertime Transport of Reactive Trace Gases From East Asia Into the Deep Tropics

Permalink

<https://escholarship.org/uc/item/59c7d3wv>

Journal

Journal of Geophysical Research: Atmospheres, 123(22)

ISSN

2169-897X

Authors

Donets, Valeria
Atlas, EL
Pan, LL
[et al.](#)

Publication Date

2018-11-27

DOI

10.1029/2017jd028231

Copyright Information

This work is made available under the terms of a Creative Commons Attribution License, available at <https://creativecommons.org/licenses/by/4.0/>

Peer reviewed



RESEARCH ARTICLE

10.1029/2017JD028231

Key Points:

- Elevated levels of anthropogenic trace gases transported in the lower atmosphere from East Asia were found behind shear lines in the deep tropical West Pacific during winter
- The chemical impact of the pollutants associated with the shear line depends on source strength, shear line organization, speed of advancement, and background conditions
- Anthropogenic Enhancement Factor is a metric developed to quantify the chemical impact of the air behind the shear line on the local background conditions

Supporting Information:

- Supporting Information S1

Correspondence to:

V. Donets,
vdonets@rsmas.miami.edu

Citation:

Donets, V., Atlas, E. L., Pan, L. L., Schauffler, S. M., Honomichi, S., Hornbrook, R. S., et al. (2018). Wintertime transport of reactive trace gases from East Asia into the deep tropics. *Journal of Geophysical Research: Atmospheres*, 123, 12,877–12,896. <https://doi.org/10.1029/2017JD028231>

Received 21 DEC 2017

Accepted 5 OCT 2018













Accepted article online 11 OCT 2018

Published online 19 NOV 2018

Author Contributions:

Conceptualization: L. L. Pan
Data curation: E. L. Atlas, L. L. Pan, S. M. Schauffler, R. S. Hornbrook, E. C. Apel, D. R. Blake
Formal analysis: Valeria Donets
Investigation: E. L. Atlas, R. S. Hornbrook, E. C. Apel, S. R. Hall, J. F. Bresch
Methodology: Valeria Donets, E. L. Atlas, L. L. Pan, S. Honomichi
Resources: L. L. Pan
Supervision: E. L. Atlas, L. L. Pan
Validation: E. L. Atlas, L. L. Pan
Writing - original draft: Valeria Donets
Writing - review & editing: Valeria Donets, E. L. Atlas, L. L. Pan, S. M. Schauffler, S. Honomichi, R. S. Hornbrook, E. C. Apel, S. R. Hall, J. F. Bresch, M. Navarro

Wintertime Transport of Reactive Trace Gases From East Asia Into the Deep Tropics

Valeria Donets¹ , E. L. Atlas¹ , L. L. Pan² , S. M. Schauffler² , S. Honomichi² , R. S. Hornbrook² , E. C. Apel² , T. Campos² , S. R. Hall² , K. Ullmann² , J. F. Bresch³ , M. Navarro¹, and D. R. Blake⁴ 

¹Department of Atmospheric Sciences, Rosenstiel School of Marine and Atmospheric Science, University of Miami, Miami, FL, USA, ²Atmospheric Chemistry Observations and Modeling Laboratory, National Center for Atmospheric Research, Boulder, CO, USA, ³Mesoscale and Microscale Meteorology Laboratory, National Center for Atmospheric Research, Boulder, CO, USA, ⁴School of Physical Sciences, University of California, Irvine, CA, USA

Abstract Unprecedented growth of East Asian economies has led to increases of anthropogenic pollutants in the regional atmosphere. This pollutant burden is transported into the global atmosphere and is a significant source of intercontinental and transboundary anthropogenic pollution. This work analyzes pollution transport into the western Pacific associated with the dispersion of East Asian pollution during Northern Hemisphere winter. To examine transport characteristics, we use chemical and dynamical data sets obtained during the CONvective TRansport of Active Species in the Tropics (CONTRAST) field campaign, conducted from Guam during January–February 2014. We identify that the evolution of shear lines from decaying cold fronts and their southward advancement facilitates polluted air transport into low latitudes of the Western Pacific Ocean. Observations from two cases of shear line passage are analyzed. The result shows that this transport process significantly elevates anthropogenic trace gases in the marine boundary layer and lowermost free troposphere up to 3–4 km. Results of our analysis show that chemical influence of the shear line on the background tropical marine atmosphere varies as a function of pollution source, intensity, shear line strength, and the speed of advancement, as well as local background conditions. To quantify the contribution of shear-line-related transport, we introduce an index, the Anthropogenic Enhancement Factor (AEF), defined as a fractional change in mixing ratio of a gas brought about by the advancing front. This index shows that the most significant enhancements are for species with photochemical lifetimes comparable to their transport times from source regions.

1. Introduction

Rapid industrialization and economic development in East Asia has been associated with a significant increase in air pollution and deterioration of local air quality. Atmospheric pollutants transported across the region also have become a significant source of intercontinental and cross-border anthropogenic pollution (Akimoto et al., 1996; Barletta et al., 2005, 2009; Lam et al., 2005; Lin, Fiore, Cooper, et al., 2012; Lin, Fiore, Horowitz, et al., 2012; Wang et al., 2014). The increasing potential of eastern and southeastern Asian regions to impact air quality locally and remotely has long been recognized. For example, the Pacific Exploratory Mission (PEM) WEST studies in the early 1990s were conducted to assess the chemistry of Asian pollution outflow into the relatively unperturbed background of the North Pacific atmosphere (Hoell et al., 1996). Investigators observed strong chemical signatures associated with oil and gas processing, various combustion sources, and industrial activities (Blake et al., 1996). Subsequent campaigns explored the chemical characteristics, geographic range, and impact of East Asian emissions on the background atmosphere. These include studies of the tropical and South Pacific (PEM-Tropics in 1996 and 1999), tropical and subtropical western Pacific Rim region (TRACE-P in 2001, BIBLE in 1998–2000, and PEACE A/B in 2002), trans-Pacific transport toward the Americas (INTEX-B, 2001), and others, which have all confirmed the persistent outflow of East Asian emissions into the background atmosphere (Blake et al., 2003). Some report increasing emissions of various pollutant gases related to rapidly accelerating economic growth (Bo et al., 2008; Hilboll et al., 2013; Kurokawa et al., 2013; Lin, 2012; Richter et al., 2005; Tanimoto et al., 2008, 2009).

Long range transport of pollution plumes from East Asia, supplemented by contributions from Europe and North America during boreal winter and spring (Pochanart et al., 2004; Wild & Akimoto, 2001), has also

received attention related to their potential for contributing to enhanced tropospheric ozone along the west coast of the United States during Northern Hemisphere spring/summer (Cooper et al., 2010; Jacob et al., 1999; Jaffe et al., 1999; Jaffe, Price, et al., 2003; Lin, Fiore, Cooper, et al., 2012; Lin, Fiore, Horowitz, et al., 2012). The springtime transport across the Pacific is also recognized as a major pathway for Asian dust dispersion (Jaffe, McKendry, et al., 2003; Price et al., 2003). Less attention has been directed to transport from Asia during other seasons, including equatorward transport into the deep tropics during the winter monsoon (Pochanart et al., 2004).

Winter meteorology in East Asia is dominated by the episodic incursions of cold air masses from Siberia into the Philippine and South China Seas. These *cold surges* (also referred to as *pressure surges*) result from the periodic drift of the Siberian-Mongolian anticyclone, affected by the passage of midlatitude synoptic waves (Compo et al., 1999; Pochanart et al., 2004). In the winter phase, cold surface temperatures give rise to stable low-level inversions that result in capping of the boundary layer. In this flow regime wet deposition is almost completely absent, which allows regional pollution to build up in the lower troposphere.

As the cold air surges are carried east-southeastward across East Asia and into the western Pacific by the prevailing westerlies, low-level pollutants originating over the continent are advected equatorward, with the strongest surges observed to advance as far south as 15°N (Compo et al., 1999; Phadnis, 2002; Lawrence & Lelieveld, 2010). As the cold air advances southward, heating from the ocean surface reduces the thermal gradient across the frontal boundary. By the time that air reaches tropical latitudes all that remains of the surface front is a wind shift referred to as a shear line. North of the shear line the formerly cold air mass should still contain the diluted pollutants entrained as the air crossed the source regions of East Asia. Anomalous climatology, such as resulting from large-scale climatic oscillations (e.g., ENSO) via perturbations of the mean wind fields, can also stimulate interhemispheric transport across the Intertropical Convergence Zone (ITCZ), entraining the pollution even further south (Avery et al., 2001).

This paper examines the atmospheric chemistry associated with these wintertime cold surges that are transported into the tropical Western Pacific. This work for the first time relates shear line development and evolution to transport of East Asian pollution into the deep tropics and attempts to quantify the effects that this transport has on the chemical composition of the troposphere in the Tropical Western Pacific (TWP).

2. The CONTRAST Experiment, Measurements and Analysis Tools

2.1. Introduction to CONTRAST

The CONvective TRAnsport of Active Species in the Tropics (CONTRAST) project was an airborne research campaign that took place in January–February 2014 using the National Science Foundation/National Center for Atmospheric Research (NCAR) research aircraft Gulfstream-V to investigate the role of convective transport in Tropical Tropopause Layer (TTL) chemistry and to measure horizontal and vertical distributions of short-lived species in the TWP (Pan et al., 2017). Operations were conducted out of Guam (13.48°N, 144.8°E), which enabled sampling of large spatial range and wide variety of photochemical environments associated with regions of deep convection to the south of Guam and the polar jet to the north.

A total of 13 research flights were performed as a part of the CONTRAST experiment. The flights covered the altitude range between 100 m above sea level up to 15 km, and the geographic area between 20°S–40°N and ~130–160°E. In addition, sampling was performed during transit flights between mainland United States to Guam and from Guam to Hawaii (Figure 1, left).

The instrument payload on the GV included a range of chemical, aerosol, and radiative instrumentation (Pan et al., 2017). The trace gas data relevant to this paper are from a subset of the payload and include measurements of reactive trace gases from a canister-based sampling system (the Advanced Whole Air Sampler [AWAS]), and an online in situ gas chromatograph/mass spectrometer Trace Organic Gas Analyzer (TOGA). We also use the high time resolution measurements of carbon monoxide (CO), methane, and actinic flux.

2.2. Organic Trace Gases

The AWAS is a canister-based gas sampling system that collects 60 samples per flight. Samples are compressed into previously evacuated 1.3 L electropolished stainless steel canisters and pressurized to

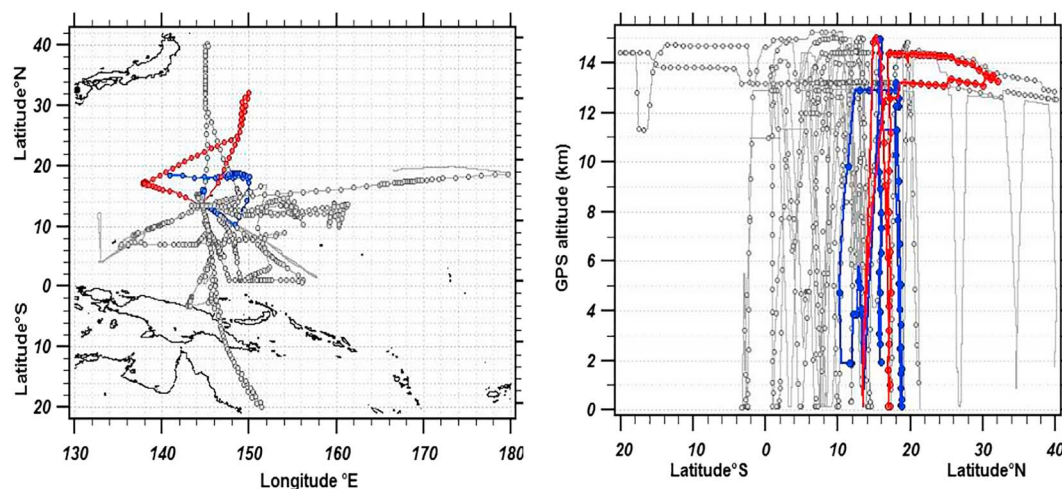


Figure 1. Horizontal (left) and vertical (right) view of CONTRAST flight tracks from research flights 1–16. Circles in both panels represent AWAS sampling locations from research flights 5–16. Research flights RF05 and RF06 are highlighted in blue and red, respectively.

approximately 3 atmospheres using 2 × 2 stage metal bellows compressors. Sample collection time in-flight ranges from 3 to 4 s at lowest flights altitudes (~100 m above sea level) to approximately 40 s at 14.5 km.

Samples were analyzed following each flight using gas chromatography with three different detection techniques: mass spectrometry (GC-MS), flame ionization (GC-FID), and electron capture (GC-ECD) to determine the mixing ratios of a large number of trace species. The analytical system was set up in a portable laboratory facility in Guam. Precision and accuracy of measured tracers vary between 2% to 20% depending on the individual compound and its concentration. Detection limits are typically in the sub-ppt to ppt level. Calibration is based on in-house and commercially prepared standards (Flocke et al., 1999; Schauffler et al., 1999). Andrews et al. (2016) discuss comparisons of trace gases measured during CONTRAST from different instruments and platforms.

TOGA is an in situ GC-MS (Apel et al., 2015). TOGA performs simultaneous measurements of all targeted gases approximately every 2 min with sample collection time of 35 s. During CONTRAST, sample volume was typically 33 ml. It uses a shock-mounted Agilent Technologies 5973 quadrupole MS system, with a modified three-stage pumping system (Apel et al., 2015). The GC is fitted with a Restek MXT-624 column (I.D. = 0.18 μm , length = 8 m). TOGA uses in-flight Zero Air/Calibration System (ZA/CS) with custom built catalytic zero air generator. Standard reference gases are from Apel-Riemer, Inc., or are prepared in-house.

TOGA precision and accuracy are compound dependent and ranges from 50% for organic nitrates to 15% for nonmethane hydrocarbons (NMHCs). Limits of detection vary from sub-ppt for NMHCs to 20 ppt for acetone and methanol.

2.3. Other Measurements

CO was measured with the NCAR Aero-Laser 5002 VUV Fluorescence with a combined uncertainty estimated at $\pm(2 \text{ ppbv} + 5\%)$ at the 2σ confidence level (similar to Gerbig et al., 1999). Methane was measured by a Picarro G1301-f Methane/Carbon Dioxide real time flight analyzer, which is based on Wavelength-Scanned Cavity Ring Down Spectroscopy with a reported 1- σ precision of 3 ppbv CH_4 for a 0.2-s integration time. Actinic flux, between 280 and 600 nm, used in the calculation of photolysis frequencies in this analysis, was measured by the High-performance Instrumented Airborne Platform for Environmental Research (HIAPER) Atmospheric Radiation Package – Actinic Flux (HARP-AF) instrument (Shetter & Müller, 1999) with a 6s duty cycle.

2.4. Satellite Data and Meteorological Analysis

The primary weather forecasting and analysis tools employed during CONTRAST were geostationary satellite products and numerical model output, both of which were obtained from the EOL CONTRAST field catalog for postproject analysis. The Japanese Meteorological Agency's MTSAT-2 (Himawari-7) provides imagery

from the visible, infrared, and water vapor channels. Observations of low cloud boundaries were often employed to indicate the locations of the shear lines and their progress.

Forecast plots from the National Center for Environmental Prediction's Global Forecast System (NCEP GFS; National Oceanic and Atmospheric Administration [NOAA] 2003) were generated at NCAR 4-time daily during CONTRAST using the 0.5-degree gridded pressure-level output. Forecast plots of surface winds, surface latent heat fluxes, and temperature were able to depict the evolution of the shear lines. In addition, numerical forecasts from the Advanced Weather Research and Forecasting model (henceforth ARW, WRF; Skamarock et al., 2008) were produced at NCAR using a 15-km grid. The higher spatial and temporal resolution of the ARW forecasts were able to resolve many of the shear lines observed during the campaign.

For our analysis we also use CO measurements obtained from the Measurements of Pollution in the Troposphere (MOPITT) instrument deployed on National Aeronautics and Space Administration (NASA)'s TERRA EOS satellite. We use Version 7 Level 3 data consisting of monthly and daily surface retrievals (combined: day and night) of CO mixing ratios from both Near and Thermal Infrared Radiances with spatial resolution of $1^\circ \times 1^\circ$.

2.5. Trajectory Calculations

To calculate air mass back trajectories, we use the 3-D Lagrangian particle advection model based on Bowman (1993) and Bowman and Carrie (2002), which is driven by 3-D winds taken from Operational Global Analysis data set supplied by NCEP. It is gridded on $1^\circ \times 1^\circ$ horizontal resolution, generated once every 6 hr, and is available on 26 pressure levels from 1,000 to 10 mb.

Using this model, we have calculated 10-day back-trajectories (utilizing 48-time steps per day) for air masses measured on two selected flights, research flight #5 (RF05, 22 January) and research flight #6 (RF06, 25 January). Results of this analysis will be presented in section 4.2 to illustrate transport pathways of reactive tracers sampled on the north side on the shear lines during these flights.

2.6. Photochemical Calculations

Mixing ratios of reactive gases emitted into the atmosphere decline as a result of atmospheric photochemical reactions, deposition to the surface, and mixing with background air. Separating the effects of mixing and photochemistry on the chemical evolution of an air mass is difficult to determine from mixing ratio measurements of a single gas (McKeen et al., 1996; McKeen & Liu, 1993; Parrish et al., 1992). However, effects of transport and dilution can be minimized by using trace gas ratios (Parrish et al., 2007; Roberts et al., 1984). The accurate calculation of *photochemical age* is predicated on a number of factors: (1) both compounds must have common anthropogenic sources with a single characteristic emission ratio, (2) species must be introduced into the air mass at the same time and removed via pseudo-first-order decay kinetics, (3) background concentrations of the trace gas in the tropospheric air must be comparatively low, and (4) the relative rates of chemical removal of the species in the hydrocarbon (HC) pair must be significantly different.

If these in the ratio between two chemical species can be related to the photochemical age of the air mass via the following relationship (equation (1)):

$$\Delta t = \frac{1}{[OH][k_A - k_B]} \times \left[\ln \left(\frac{[A]}{[B]} \right)_{t=0} - \ln \left(\frac{[A]}{[B]} \right) \right] \quad (1)$$

where

- Δt = is the photochemical age;
- k_x = rate constant for OH oxidation of compound x;
- [OH] = average OH radical concentration;
- [A], [B] = atmospheric mixing ratios of two species, where $t = 0$ represents mixing ratios of gases at the source.

A few important caveats to this approach include the uncertainties related to source mixing ratios of the chosen chemical species (Factor 1), as well as the assumption of the negligible effects of mixing and dilution. While uncertainty due to Factor 1 might be minimized by averaging regional data, additional information in the form of back trajectory analysis, for example, might help in explaining differences in separate cases

of long-range transport (i.e., based on the air mass trajectory for isolated cases of long-range transport using regional averages may not be an appropriate metric). Similarly, effects of mixing and dilution cannot be completely ignored either. McKeen and Liu (1993) demonstrated that atmospheric mixing significantly affects not just individual chemical species, but ratios of chemical species as well, and ratios themselves therefore represent the combined effects of photochemistry and mixing (see section 4.2.1. for further discussion).

HC species with lifetimes characteristic of regional (<4 days) and intercontinental (<30 days) transport time scales are the most suitable chemical tracers for the method described above. For example, toluene and benzene satisfy the constraints of the method by sharing common anthropogenic origins (related to incomplete fuel and industrial combustion and solvent evaporation) (Apel et al., 2010, 2012; Barletta et al., 2009; Blake et al., 2003), following the same first-order gas-phase kinetics with their primary oxidation mechanism being reaction with hydroxyl radical (Wang et al., 2013; Wu et al., 2014), and reacting at rates significantly different from each other. For CONTRAST conditions, the photochemical lifetimes are approximately 2 days for toluene (T) and 10 days for benzene (B). Light alkane pairs of faster reacting HCs, such as the C_4/C_3 , C_5/C_3 , and C_6/C_3 with approximate lifetimes of $C_3 = 13$ days, $C_4 = 6$ days, $C_5 = 3$ days, and $C_6 = 2$ days can also be used, especially for transport timescales of 1–1.5 weeks.

Based on our assessment of the available measurements over source regions in question, we chose T/B and C_5/C_3 HC pairs for our analysis. Rate constants used in the calculation are from Perry et al. (1977), Atkinson (2003, 2007), and Burkholder et al. (2015) and were adjusted to modeled temperature utilizing back trajectory data with the assumption of 24 hr average hydroxyl radical concentration of 10^6 to account for latitudinal gradients of OH during boreal winter, ranging from 0.7×10^6 to 3×10^6 (Carpenter et al., 2014; Patra et al., 2014).

3. Observations

3.1. Meteorological Background of Two Selected Flights

Products from NCAR MMM WRF-ARW (supplemented by products from Taiwan's Central Weather Bureau operational Advanced Research WRF; Skamarock et al., 2008) and local satellite images were used for forecast and flight planning during the campaign. The specific products used to trace the evolution of the shear lines and depict their location at the time of sampling include Surface Latent Heat Flux and Surface Wind products at 20-km horizontal resolution, the ARW Surface Latent Heat Flux and Surface wind and Temperature products at 15-km resolution, and a series of MTSAT-2 Channel-1 Visible images.

We will concentrate on two research flights of CONTRAST field campaign that sampled chemical gradients associated with two consecutive shear line passages through the research domain; these are designated RF05 (22 January 2014) and RF06 (25 January 2014). The surface cold front that evolved into the shear line sampled during RF05 moved off the Asian continent late on 17 January. A surface cyclone along the front deepened rapidly as it moved from 33°N, 145°E on 18 January to near 45°N, and 175°E on the 20 January (not shown). The strong northerlies west of the cyclone helped drive the cold air mass southward to near 20°N late on 19 January (Figure 2; left panels) As the surface low continued eastward on 21 January remnants of the cold front persisted as a weak, shear line extending from the Philippines to the center of the surface low, with winds on the north side of the shear line from the east-northeast at 10–15 m/s and from the east at 5 to 10 m/s south of the shear line (Figure S2c). Convection associated with a tropical disturbance moved from southeast to northwest over Guam late on 21 January and interacted with the shear line north of Guam. The shear line persisted at 0 UTC on 22 January, approximately 6 hr in advance of sampling; however, it had weakened with winds diminishing to about 5–10 m/s in most areas (not shown).

The shear line associated with RF06 evolved similarly to the RF05 case but was more intense. As a surface cyclone traversed Japan on 20 January, it trailed a cold front from near 38°N, 145°E to 25°N, and 120°E. As the surface cyclone moved east-northeast it deepened rapidly and drove the cold air southeastward across the west Pacific toward Guam. By 0 UTC 23 January the cold front started making its way into the research domain. The leading edge of the cold air mass retained frontal characteristics including temperature decreases and a pronounced shift in the wind direction and much stronger wind velocities between 15 and 20 m/s just northwest of Guam.

By 0 UTC 24 January southward progress of the front had slowed north of Guam as it transitioned to a shear line. The shear line was characterized by 10–15 m/s surface winds to the north of the line and a well-defined

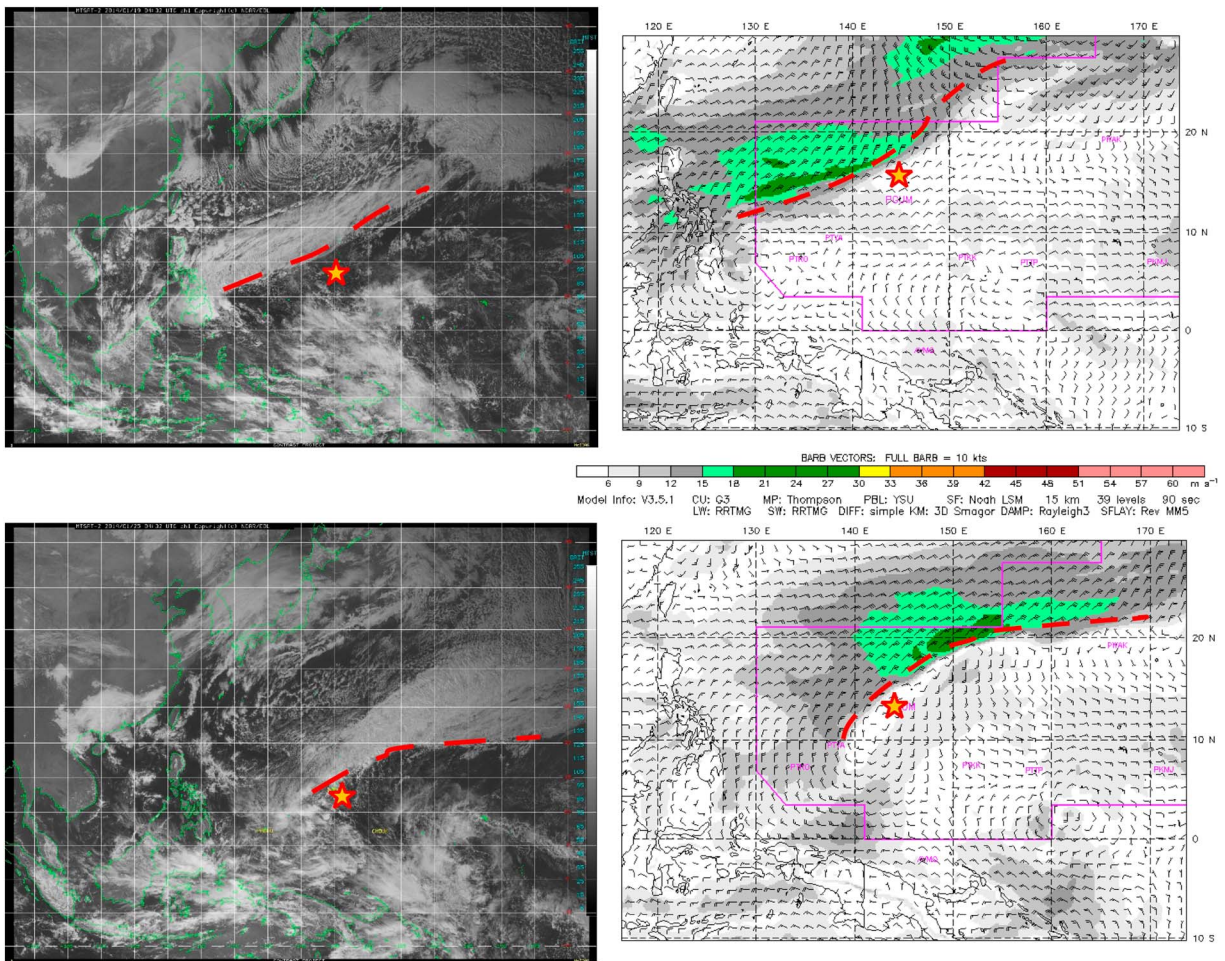


Figure 2. Japanese Meteorological Agency’s (left) MTSAT-2 visible channel imagery for (top left) the 19 January and (bottom left) the 25 January showing the organization of shear lines sampled during RF05 and RF06, respectively, with corresponding horizontal surface wind speeds calculated from the 15-km resolution NCAR/MMM WRF-ARW at the top right (RF05) and bottom right (RF06). Approximate shear line locations are indicated with red dashed lines; Guam is marked with a star. The two bottom panels show the state of the shear line sampled during RF06 an hour before interception on the 25 January, while the top panels show shear line organization 3 days prior to RF05 sampling on the 22 January, when the shear line sampled during RF05 was most organized. The purple line in the NCAR/MMM WRF-ARW images is the Oakland FIR boundary.

horizontal directional wind shift. On 25 January the shear line persisted just north of Guam, with winds in 15–20 m/s range. The location of the shear line was also evident from MTSAT-2 visible channel imagery, where the boundary can be recognized from the presence of cumulus congestus produced as a result of frontal convective lifting (Figure 2; bottom right panel).

3.2. Chemical Measurements

The 717 whole air samples collected during research flights 05–16 along with vertical distribution of those samples are presented in Figure 1 (no data is available for RF01–RF04 due to sample inlet problems). Highest density of sampling occurred between ~4–20°N (Pan et al., 2017) and ~135–155°E; however, higher altitude excursions north and south also allowed sampling of the polar jet ~40°N and Southern Hemispheric tropical air masses ~20°S. Table S3 and Figure 3 (collapsed subset) show mixing ratios of selected trace gases (including mean, median, and standard deviation) obtained from AWAS, TOGA, and Aerolaser 5002 (CO) instruments. Measurements are averaged in 2-km vertical bins, from boundary layer (<2 km) to the lowermost TTL (above 14 km). We compare those measurements to the data collected during phase B of the PEM-WEST (P-WB) experiment (February–March 1994) and TRACE-P (T-P) campaign (February–April 2001) that also surveyed a portion of the Western Pacific, however with efforts largely concentrated in the area nearer to the Pacific Rim region (Blake et al., 2001). We only select P-WB and T-P measurements that overlap with the CONTRAST research domain.

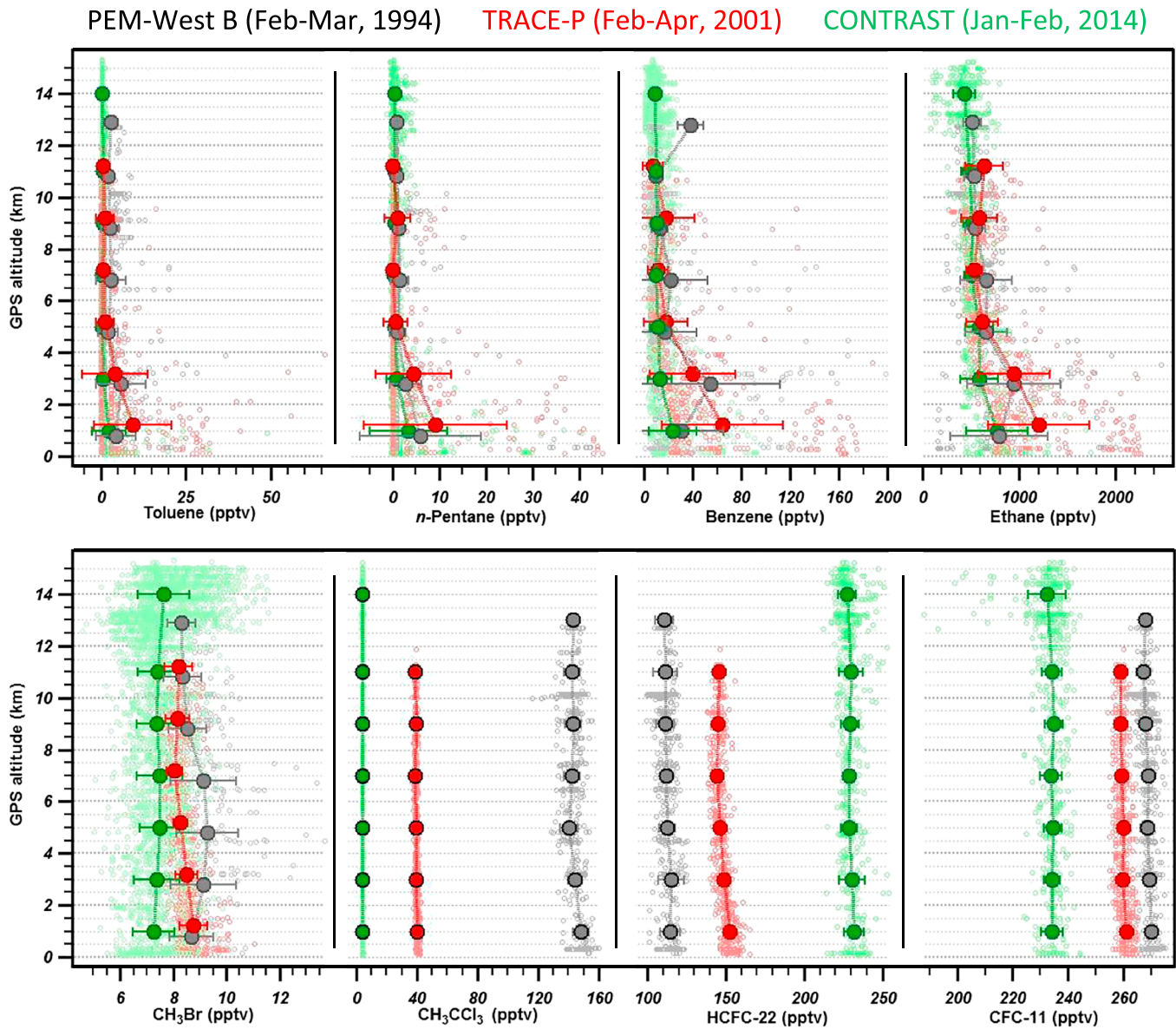


Figure 3. Vertical profiles of selected volatile organic compounds measured during PEM-West B (grey), TRACE-P (red), and CONVECTIVE TRANSPORT OF ACTIVE SPECIES in the Tropics (CONTRAST) (green). Profiles are plotted in 2-km altitude bins (large filled circles), with small open circles showing all measurements taken within specified research domain. Horizontal bars represent one standard deviation of the averages within each vertical 2-km bin.

In comparison to previous measurements carried out in the TWP, in particular T-P, on average, CONTRAST sampled cleaner air masses. Median mixing ratios of oxygenated volatile organic compounds (OVOCs) encountered during CONTRAST (excluding formaldehyde) were significantly lower throughout the entire tropospheric column, with CONTRAST measurements averaging 10 times lower than T-P in some free troposphere (FT) measurements. Boundary layer NMHC measurements during CONTRAST were slightly lower than P-WB values, while FT values were about twice as low and ~1.5 times lower in the region above 8 km. T-P values on the other hand were on average ~2 times higher than during CONTRAST throughout the entire tropospheric column. Measurements of aromatic HCs (benzene and toluene) were also generally lower in CONTRAST samples.

In comparing CONTRAST to P-WB and T-P, we observed significantly lower mixing ratios of a number of chlorinated solvents (e.g., carbon tetrachloride [CCl₄], methyl chloroform [CH₃CCl₃], and tetrachloroethylene [C₂Cl₄]) and CFCs and Halons (e.g., CFC-11 and Halon-1211), mostly resulting from phasing out the

production of these substances under the Montreal Protocol and decreased use. Mixing ratios of a number of hydrochlorofluorocarbons (HCFCs; HCFC-22, HCFC-141b, and HCFC-142b) and long-lived CFCs (e.g., CFC-114) however have been steadily increasing in the TWP from 2000 to 2014. These trends are consistent with surface mixing ratios of these gases measured at ESRL and AGAGE stations, though AGAGE data show a small decrease in CFC-114 (0.3 ppt) from 2004 to 2017 (Prinn et al., 2000). For CONTRAST, measurements are in reasonable agreement with the NOAA ESRL GMD station data in Mauna Loa, Hawaii (MLO), and Guam (GMI), especially for halocarbons. Shorter lived HC data obtained during CONTRAST are on the lower range of MLO and GMI measurements (Helmig et al., 2017).

While on average CONTRAST observed lower mixing ratios of many trace gases compared to earlier measurements in the region, a significant variability in tracer mixing ratios was observed in the course of the campaign. In Figure 4, we compare the vertical profiles of five volatile organic compounds (VOCs) and CO from all measurements reported for CONTRAST (AWAS: RF05-RF16; TOGA: RF02-RF16; and CO: RF03-RF16) to vertical distributions of the same tracers observed during the two flights featuring shear line passages (RF05 and RF06). A selected subset of gases, including toluene (C_7H_8), n-pentane ($n-C_5H_{12}$), benzene (C_6H_6), chlorobenzene (C_6H_5Cl), ethane (C_2H_6), CO, methyl bromide (CH_3Br), and CFC-11 (CCl_3F), were chosen to represent a wide variety of anthropogenic source types and lifetimes. Relative to the rest of the CONTRAST data set, measurements obtained during RF05 and RF06 clearly represent some of the highest mixing ratios measured during the campaign, particularly in the lower troposphere. Tracers showing greatest enhancements are those associated with industrial activities, including metal degreasing, petroleum refining, and synthesis manufacturing (solvents and non-methane volatile organic compounds), inefficient combustion of bio-fuels and fossil fuels (NMHCs and OVOCs), and general urban emissions (HCs, CO, etc.). These increased mixing ratios during RF05 and RF06 highlight the potential importance of the shear lines as the boundary of a polluted, continental air mass. Gradual change of tracer profile shapes as a function of their atmospheric lifetime is also a notable feature, with longer lived species exhibiting more uniform vertical distributions.

4. Analyses

4.1. Trace Gas Data

A wide variety of chemical tracers can be used to investigate potential origins and photochemical processing of air masses transported to a remote location. During transport physical processes of convection and mixing with ambient air, wet/dry deposition, and secondary photochemical production progressively modify the chemical makeup of the air mass. To interpret the chemical signatures within an air mass, it is best to examine a wide variety of species while considering effects of both, transport and photochemistry. While emissions of trace gases of both natural and anthropogenic origin contribute to the composition of remote air masses, we limit our analysis here mostly to trace gases produced anthropogenically, omitting analysis of biogenic tracers with predominantly terrestrial and/or oceanic sources. The set of anthropogenic trace gases considered here provides the clearest contrast between their well-defined sources and the remote atmosphere of the TWP. (See Table S1 for full list of tracers used in the analysis.)

In the first part of the discussion we examine vertical profiles of trace gases from two selected flights (RF05 and RF06) that are associated with air mass transport and focus on enhancements in mixing ratios of anthropogenic tracers in the boundary layer and lower FT (up to ~4 km). For each of the flight profiles, we use a suite of organic trace gases to demonstrate the contrast between the relatively unperturbed, aged air characteristic of tropical Pacific atmosphere, and the polluted air transported to the region.

Two groups of comparisons are made to help quantify the trace gas enhancements associated with the migrating shear lines. Figure 5 shows the first group of comparisons using probability density functions of six selected trace gas data in the lowermost 4 km. In Figure 5, the RF05 and RF06 measurements in the profiles ahead of the shear lines (designated as *reference* profiles) are compared to all CONTRAST measurement within lowermost 4 km. This comparison is made to provide a qualitative perspective of the amount of the selected species in the reference profiles in RF05 and RF06 relative to the TWP background. These species are selected to represent a wide spectrum of atmospheric lifetimes (from 2 to 3 days for toluene to just under a year for methyl bromide) to demonstrate a likely lifetime dependence in the enhancements. Despite the fact that number of data points available from RF05 exceeded that of RF06, all distributions show a

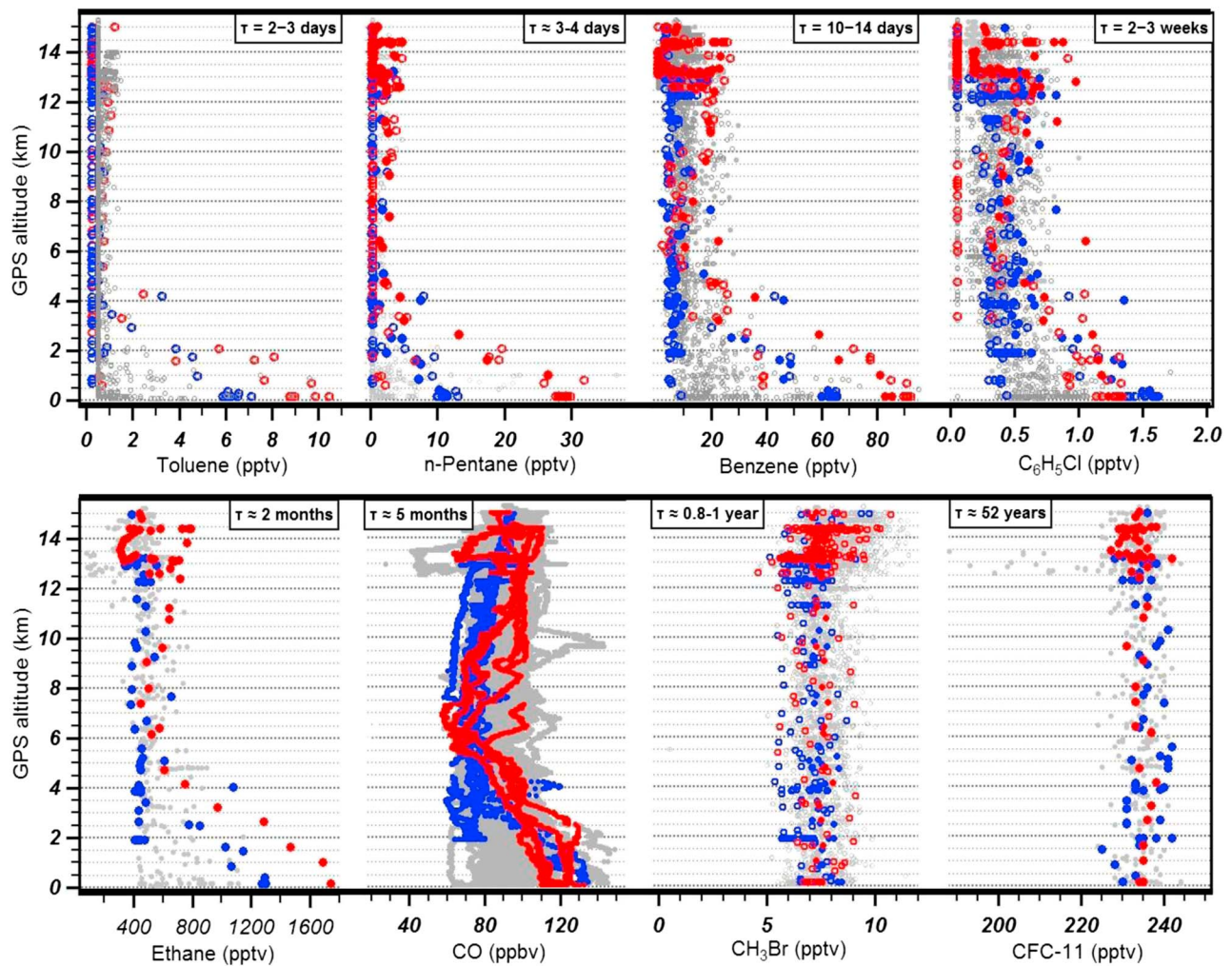


Figure 4. Vertical profiles of selected volatile organic compounds and CO during the CONvective TRansport of Active Species in the Tropics (CONTRAST) research campaign. Highlighted data are from RF05 (blue) and RF06 (red). The filled circles represent data collected using Advanced Whole Air Sampler (AWAS) instrument, the open circles are from Trace Organic Gas Analyzer (TOGA) instrument. Carbon monoxide profiles represent high-frequency data set from the CO-VUV instrument at 1-s resolution.

consistent trend for defining the background conditions: RF05 shows peaks at lower mixing ratios compared to the entire campaign data, while RF06 data are shifted to higher mixing ratios. In the case of RF05, averaged measurements from profiles taken in front of the disintegrating shear line (south of the shear line) were among the lowest collected during the research campaign and therefore could be considered as a proxy for near background tropospheric values of the TWP, during CONTRAST mission period.

The second group of comparisons is shown in Figure 6, where the profiles of benzene and toluene measured ahead and behind the shear lines are compared for RF05 and RF06, respectively. The large differences in the mixing ratios of both tracers between the polluted and the reference profiles in the lowermost 4 km highlight the significant pollution transport associated with the migrating shear lines.

When comparing the two flights, the RF05 is found to contain lower mixing ratios of anthropogenic tracers overall than the measurements in RF06, but the ratio of *polluted* to *background* trace gas concentrations were higher during RF05 (see section 4.3; Figure 3s).

Although not shown in figures, high mixing ratios of CO (in excess of 125 ppbv) and anthropogenic trace gases north of the shear line in both RF05 and RF06 represented the most polluted conditions during the entire campaign. For example, mixing ratios of NMHCs during RF06 were the highest measured in the entire domain. Similar trend can be observed in mixing ratios halocarbons originating from solvent

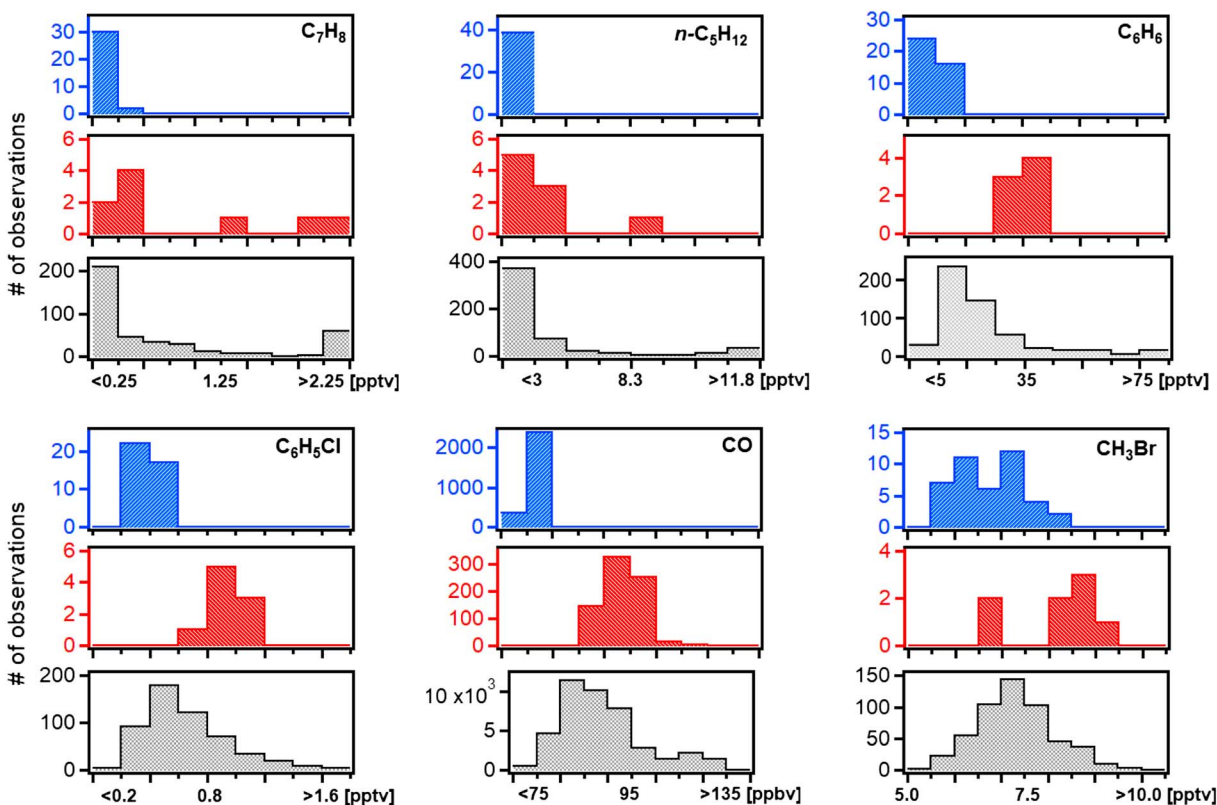


Figure 5. Probability density function plotted for selected volatile organic compounds and carbon monoxide. Data in gray represent all CONvective TRansport of Active Species in the Tropics measurements under 4 km, while blue and red represent RF05 and RF06 reference profile (background) measurements (similarly <4 km), respectively.

evaporation, e.g., tetrachloroethylene (C_2Cl_4), 1, 2-dichloroethane [$C_2H_4Cl_2$], chlorobenzene [C_6H_5Cl], carbon tetrachloride [CCl_4], and methylene chloride [CH_2Cl_2], with values measured during RF06 and RF05 being highest of the campaign for the first 3 compounds listed.

Significant enhancements of OVOC tracers strongly correlated with both NMHCs and CO north of the shear line in RF05 and RF06 were also observed, suggesting continental and predominantly industrial and urban emission sources (Ashfold et al., 2015; Gregory et al., 1996; McCulloch et al., 1999).

Overall, the anthropogenic emission tracer enhancements observed during CONTRAST were found predominantly in the shorter lived (lifetimes of days to a few months) gases. Longer lived trace gases maintained a uniform vertical profile, with no measurable enhancements in the lower troposphere. This behavior will be analyzed in more detail in section 4.3.

4.2. Results of Photochemical Age Calculations, Back Trajectory Analysis, and Wintertime MOPITT Data

In this section we combine the results of kinematic back trajectory analysis and calculations of photochemical ages to characterize air masses sampled during RF05 and RF06 and to identify potential locations of source emissions. We will first assess the impact of the well-organized shear line sampled during RF06, where measured concentrations of trace gases significantly exceeded those during RF05, followed by a discussion of impacts that shear line passages have on the background conditions characteristic of Western Pacific atmosphere, using the RF05 case as an example.

For the necessary starting conditions of our photochemical age calculations, we use a combination of VOC data from a variety of locations throughout China, Japan, and South Korea, including ESRL station data. We

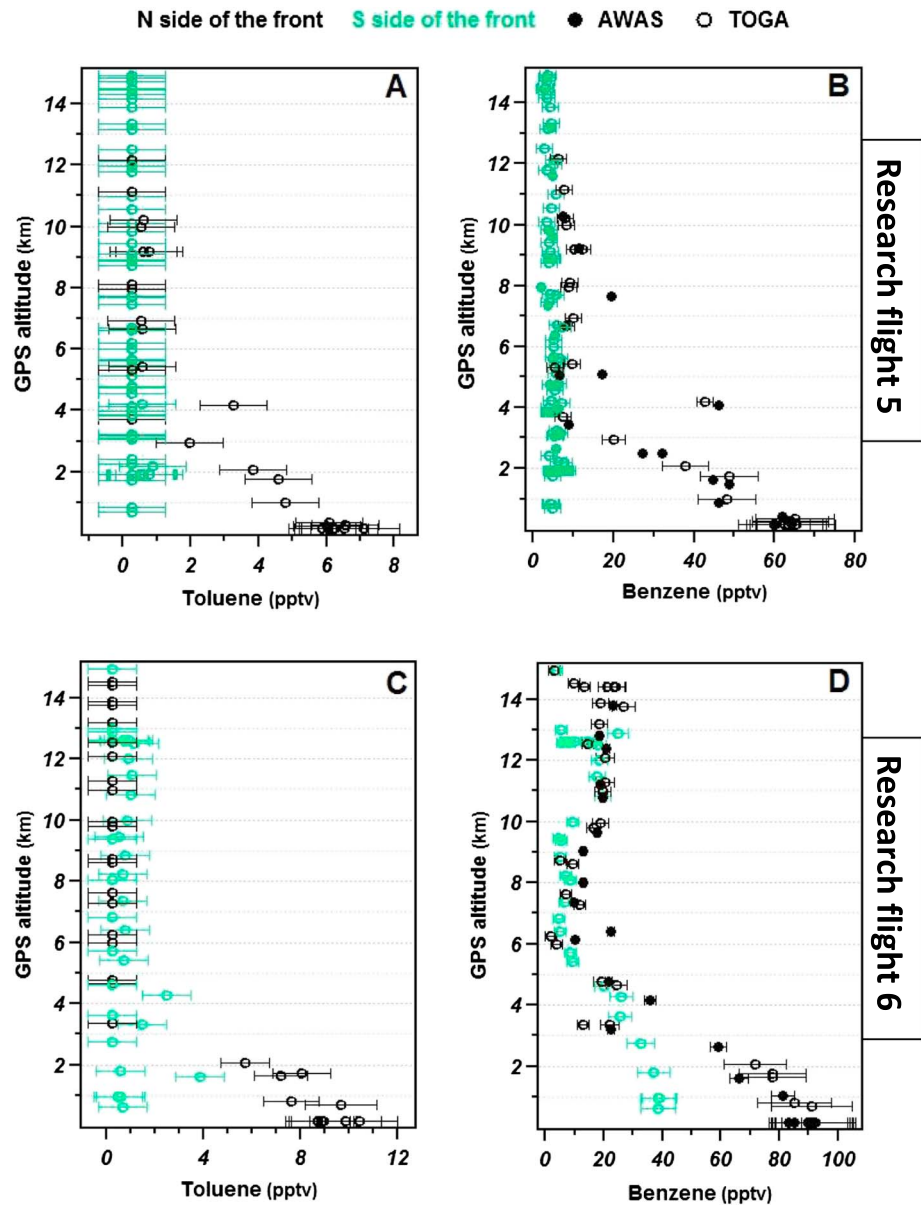


Figure 6. Vertical profiles of benzene and toluene mixing ratios for flights (top) RF05 and (bottom) RF06. Measurements on the south (unpolluted) side of the migrating shear line are plotted in green symbols. The black symbols are measurements from the north (polluted) side of the shear line. Advanced Whole Air Sampler (AWAS) data are plotted in filled circles, and Trace Organic Gas Analyzer (TOGA) data are shown as open circles. The error bars show the reported uncertainties.

choose only winter and early spring season measurements to represent source emission ratios for our calculations (see Table S5 for full description of source mixing ratios).

4.2.1. Analysis of the Chemical Enhancements and Photochemical Age Calculations for RF05 and RF06

As noted earlier, vertical profiles north of the advancing shear line during RF06 displayed marked increases in mixing ratios of reactive trace gases in the lowest altitudes (>800 hPa; <2 km; Figures 6c and 6d). Air in this lower altitude region featured an average 14-fold increase in mixing ratios of NMHCs, 5-fold increase in mixing ratios of aromatic HCs, a 2-fold increase in mixing ratios of OVOCs, and further and variable increases in other tracers associated with anthropogenic emissions (Table S2) compared with background conditions ahead of the shear line. Similar to RF06, on the north side of the dissipating shear line boundary during RF05, enhancements in pollutant trace gases in the lowermost parts of the profile (>700 hPa;

Table 1
Estimates of the Photochemical Ages of the Air Masses Intercepted on the North Side of the Shear Line During Flights RF05 and RF06

Source	Research flight 5		Research flight 6	
	C ₇ H ₈ /C ₆ H ₆	n-C ₅ /C ₃	C ₇ H ₈ /C ₆ H ₆	n-C ₅ /C ₃
China				
Barletta et al. (2005)	5.6		3.9	
Zhang et al. (2012)	5.5		3.9	
Li et al. (2014)	3.2		1.5	
Li et al. (2015)	5.4	8.3	3.8	5.7
Wang et al. (2016)	5.1		3.4	
Jia et al. (2016)	3.5	9.9	1.9	7.4
Zhang et al. (2017)	3.8		2.1	
Liu et al. (2017)	4.8	5.9	3.2	3.3
Gao et al. (2018)	5.8	7.0	4.1	4.4
	4.7 ± 1.0	7.8 ± 1.7	3.1 ± 1.0	5.2 ± 1.8
Japan				
Kagawa et al. (2005)	4.9		3.0	
Ohura et al. (2006)	8.7		7.0	
Shirai et al. (2007)	8.3	6.0	6.7	3.5
Morino et al. (2011)	9.7	4.1	8.1	1.5
Uchiyama et al. (2015)	7.4		5.7	
	7.7 ± 1.8	4.1 ± 1.3	5.9 ± 1.9	2.5 ± 1.4
South Korea				
Na et al. (2002)	6.7	10.2	5.1	7.6
Lee et al. (2005)	8.3		6.6	
Kim et al. (2008)	9.6		7.9	
Byeon et al. (2010)	5.7		4.0	
Anmyeon-do (AMY), ESRL 2014		8.0		3.5
Tae-ahn Peninsula (TAP), ESRL 2014		11.0		8.6
	7.6 ± 1.7	9.7 ± 1.6	5.9 ± 1.7	6.6 ± 2.7
	7.0 ± 1.8		4.8 ± 1.6 days	

Note. Calculations are based on toluene/benzene (T/B) and n-pentane/propane (n-C₅/C₃) ratios, using combinations of wintertime volatile organic compound measurements from China, Japan, and South Korea for starting mixing ratios.

South Korea (~4) and Japan (~6), which in turn results in differences in calculated photochemical ages. The same is true for n-C₅/C₃ calculations with ratios being lowest for sources in Japan (0.09), slightly higher based on source mixing ratios measured in China (0.1), and highest over South Korea (0.3). This regional variability of source composition and uncertainty in specific source regions contributes uncertainty to the calculated photochemical ages, as mentioned in section 2.6.

As well as the uncertainties in the source mixing ratios, the influences of mixing and dilution cannot be completely eliminated. Three different scenarios should generally be considered: (1) injection of freshly emitted HCs into the air parcel from other sources during transport, (2) mixing with background air, and (3) dilution with air, containing partially aged HCs. Based on the back trajectory analysis, scenario (1) is unlikely, as in case of both flights air parcels rapidly move away from the continental landmass, and continue on the trajectory away from major source regions. Options (2) and (3) on the other hand present more likely scenarios. In both cases, dilution by more aged HCs will cause photochemical *clocks* since the last encounter with a fresh source to run faster, affecting more reactive HC to the lesser extent than the more reactive one out of the pair (Parrish et al., 1992). Parrish et al. (2007) showed that the evolution of ratios of fast reacting alkanes (C₃-C₆) resulted in strongly kinetic behavior, while aromatic ratio relationships showed rather strong deviations from it, attributed to the effects of mixing. This implies that the photochemical age calculations based on the T/B benzene ratio may contain a stronger *mixing bias*, compared to the calculation utilizing C₅/C₃ HC pair, but in both cases estimated ages would be shorter times if mixing parameterization is included.

<2.5–3 km) were observed (Figures 6a and 6b). Chemical gradients across the shear line boundary during RF05 were stronger than those observed during RF06 (30-time average increase in NMHC mixing ratios, 10-time increase in aromatic HCs, and 4-time increase for OVOCs), despite the fact that concentrations of tracers on the north side of the front were lower than during RF06. The different chemical gradients we observed in the two flights are related to the meteorological conditions represented by the reference profiles in the two flights. South of the dissipating frontal boundary during RF05 was an area of active convection. During RF05 a weak cross-equatorial flow was established with southeasterly winds prevailing in the area where the reference profile was sampled. Embedded in that flow, a mesoscale convective system was moving over Guam with ozone showing strong signs of convective control (Pan et al., 2015). These conditions led to a very well mixed reference profile typical of the remote tropical atmosphere. Reference profiles sampled during RF06, on the other hand, still contained diluted pollutants in the BL and lowermost FT left over from previous shear line passage on the 22 January.

For each flight, we use measurements of toluene, benzene, propane, and n-pentane on the north side of the advancing front averaged over lowermost 1 km (<900 hPa), where the largest enhancements were observed, to represent mixing ratios at time = *t*, required in equation (1) (section 2.5). Results of these photochemical age calculations are presented in Table 1. Calculations suggest a faster transport of pollutants from the source of emission in the case of RF06, compared to the RF05, with photochemical age of 4.8 ± 1.6 and 7.0 ± 1.8 days for RF06 and RF05, respectively.

It should be pointed out that calculated photochemical ages vary regionally due to the differences in estimated source emissions from China, Japan, and South Korea. T/B source ratios over China are systematically lower (~1), than those based on data from

4.2.2. Back Trajectory Analysis and Consistency With MOPITT Observations

Differences in mixing ratios across the shear line boundaries observed during both flights suggested different origins of the air masses to the north and south of the shear line, as well as within the profile itself. The calculated back trajectories for RF05 and RF06, generated between the surface and 10 hPa at 5-s intervals, are presented in Figure 7.

For RF06, back trajectories generated along the flight track within the vertical profiles north of the shear line (17°N, 138°E) confirmed different air mass histories for samples below 800 hPa (where enhancements of reactive trace gases were observed) and the FT above 3 km, which closely approximated background levels. In the RF06 case three different pathways can be identified. The first pathway includes parcels arriving at the flight track at 400 hPa and above which seem to originate at <400 hPa over portions of continental Southeast Asia and <250 hPa over tropical western and central Pacific. The second pathway includes parcels arriving at the flight track between 750–400 hPa from W-NW. These parcels also show anticorrelated CO and ozone, which suggests some degree of mixing with stratospheric air. Finally, the third pathway contains air parcels sampled below 800 hPa. These parcels are embedded in the midtropospheric westerly flow carried over from central and northern Asia, as shown by the 7-day (and 10-day) back trajectory analysis (see Figure S3. for extended 10-day back trajectories). These trajectories reach the nearest potential source region in Japan at -3 days. From Japan, the air mass rapidly proceeds toward the tropics, wrapping around an intensifying anticyclone to the west.

Back trajectory analysis for the chemically perturbed profile during RF05 follows a generally similar flow pattern to RF06 (with the exception midtropospheric parcels between 400 and 700 hPa passing over India in RF06). Trajectories for RF05 can be divided into two categories based on their source region. Trajectories generated for air parcels sampled at <700 hPa represent a portion of air with a clear marine source, originating from the MBL and lower (>500 hPa; <5 km) FT of the central Pacific. This air had been trapped in a persistent surface anticyclone and was convectively uplifted with the passing mesoscale convective system. Parcels originating >700 hPa in the measurement profile represent surface continental sources. Based on the trajectory model, parcels originate at high levels (<500 hPa) in areas of northern and central Asia, as well as the area north of Japan over the Sea of Okhotsk. As trajectories are carried with the north-westerly flow, they start descending toward the surface (>600 hPa; <3.2 km), while approaching heavily industrialized areas of NE China, North and South Korea, and southern and central Japan approximately 6 days before sampling during RF05. At T-5 days, trajectories from central Asia merge with trajectories from the Sea of Okhotsk just off the coast of Japan, and they make their way to the research domain over the next 4 days, being steered by eastward moving low and high pressure systems.

Areas of East Asia where trajectories interact with the continental landmass, also corresponds with the high levels of CO from MOPITT observations from >900 hPa. CO mixing ratios are in the 130–200 ppbv range over central and northern Japan and further west over southern Siberia toward Kazakhstan, as well as well in excess of 200 ppbv in the regions around NE China, and SE Russia, where parcel trajectories are indicated to flow within the lower FT, below 500–600 hPa (Figure 8).

Summarizing dynamical and photochemical data sets from the two flights, we observe similar patterns of air mass movement with consistent origins and sources in urbanized areas of eastern and northern Asia. The different impact between the two cases appears to be modulated by the speed and strength of shear line progression. Both dynamical and chemical analyses of the RF06 data indicated a quicker transport of polluted air toward the tropical western Pacific. The faster transport explains the higher mixing ratios of the reactive gases that were measured, as the air mass had less time for photochemical degradation and mixing.

4.3. Relationship Between Transport Time and Enhancement Factor of Trace Gases

In this section we use the trace gas observations from RF05 and RF06 to investigate a relationship between the chemical gradients of reactive trace gases across the frontal boundary, their photochemical lifetimes, and the calculated transport times from their emission sources. To accomplish this, we introduce the notion of an Anthropogenic Enhancement Factor (AEF), defined as a fractional change in mixing ratio of a trace gas between environments that are affected versus unaffected by the shear line. The AEF is calculated by equation (2):

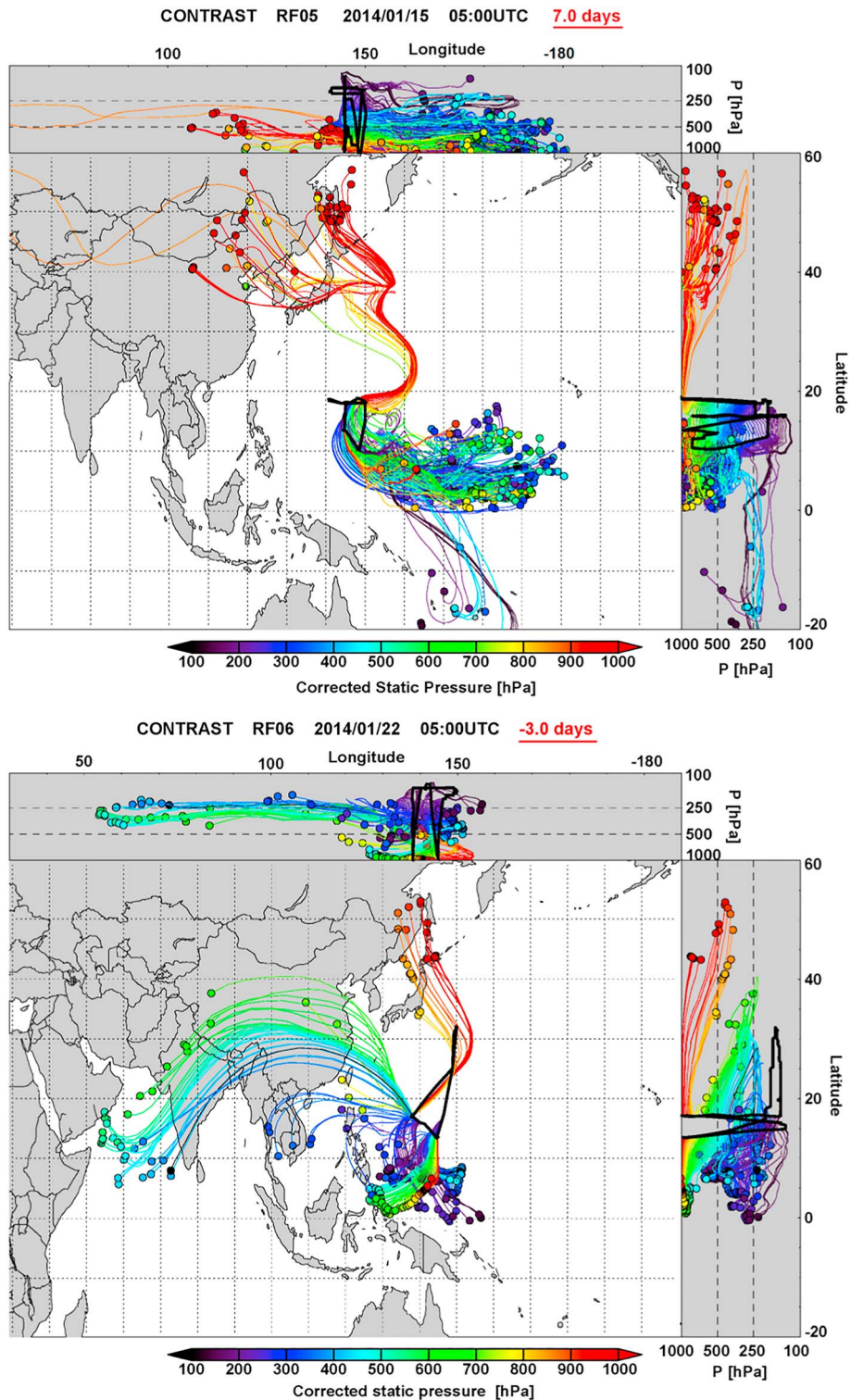


Figure 7. Seven-day back trajectories for RF05 (top) and 3-day back trajectories for RF06 (bottom) from locations along the flight profiles on the north side of the shear line, color-coded by the initial pressure during the profile measurement. Top panel for each set of trajectories shows the altitude-longitude sections, with the same color coding. Right side panels on each illustrate the latitude pressure cross sections. The trajectories displayed are computed every 5 s along the flight track, and every third trajectory is plotted (see supporting information Figure S2 for longer-period back trajectories).

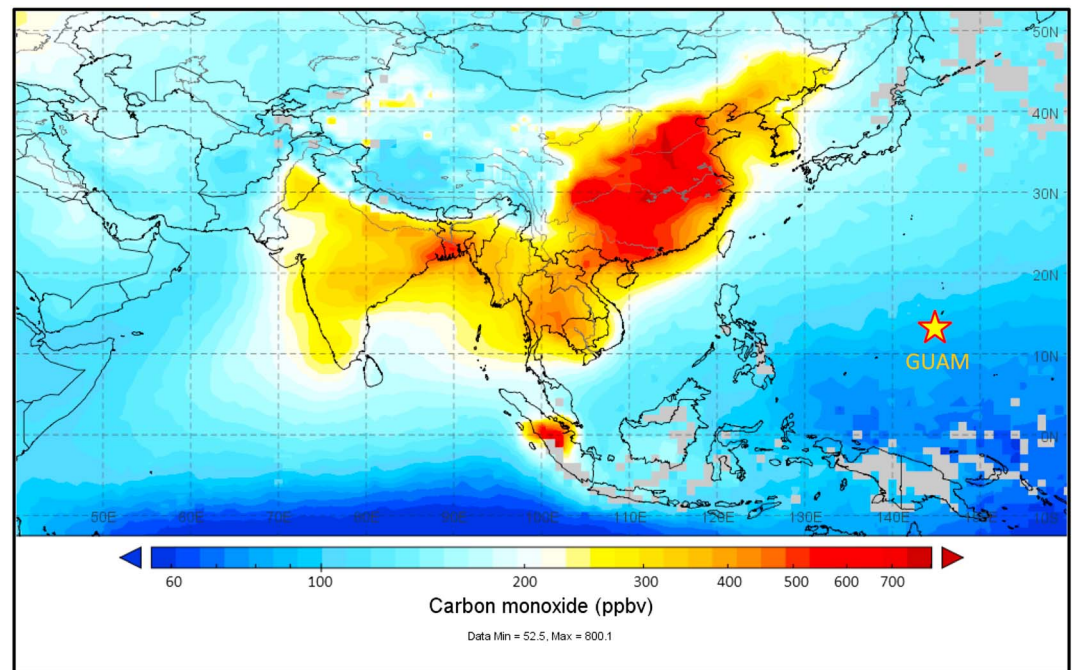


Figure 8. Measurements of Pollution in the Troposphere (MOPITT) retrieved surface layer (>900 hPa) mixing ratios (day and night combined) from January 2014, utilizing both thermal and near-infrared radiances (Deeter et al., 2017). Mixing ratios in excess of 400 ppbv over industrialized areas of eastern and southeastern Asia, with areas to the north, east, and west in the 200-ppbv range.

$$AEF = \left(\frac{N_b - N_f}{N_f} \right) \quad (2)$$

where:

N_b – mixing ratio of a gas behind the shear line (polluted side of the frontal boundary);

N_f – mixing ratio of a gas in front of the shear line (unaffected environment).

For this analysis we are only concerned with gases having predominantly anthropogenic sources, with low secondary production potential (OVOCs are rejected on this basis). We group these gases into lifetime ranges and then average the calculated enhancement factor across all gases assigned to the same lifetime bin. Despite the meteorologically driven differences between the two flights, we are assuming 7.0 ± 2.0 day transport from source to the location of the measurement for RF05 and 4.7 ± 1.9 days for RF06, as established earlier using calculations of photochemical aging, though trajectory calculations suggest a potentially younger age for RF06 of approximately 3 days. The overestimate from our photochemical clock approach is expected to result from mixing of the gases in the polluted air mass with nonzero background concentrations (as discussed in section 4.2.1).

Both cases show a unimodal distribution with well-distinguished peaks. RF06 shows highest AEFs for tracers with photochemical lifetimes between 3 and 4 days, and the RF05 AEF distribution maximizes for compounds with lifetimes of 5–6 days (Figure 9), falling within a range suggested by both back trajectory model and chemical estimates of the age.

The AEF distribution has useful and interesting information. For both flights, the peak of the AEF distribution does not fall on the very short or very long-lived species. It is clear that the AEFs will maximize very early in the transport history for trace gases with short lifetimes and will remain small for trace gases with long lifetimes and relatively small emissions. For those with medium lifetimes (days to weeks), however, the AEFs will depend on emission intensity, transit time, and definition of N_f (mixing ratio of a trace gas in the background atmosphere, here represented by the measurement ahead of the advancing front).

With an appropriate choice of N_f in a theoretical case utilizing an idealized photochemical loss function, the above relationship results in an AEF of any particular trace gas maximizing at a transport time similar to the

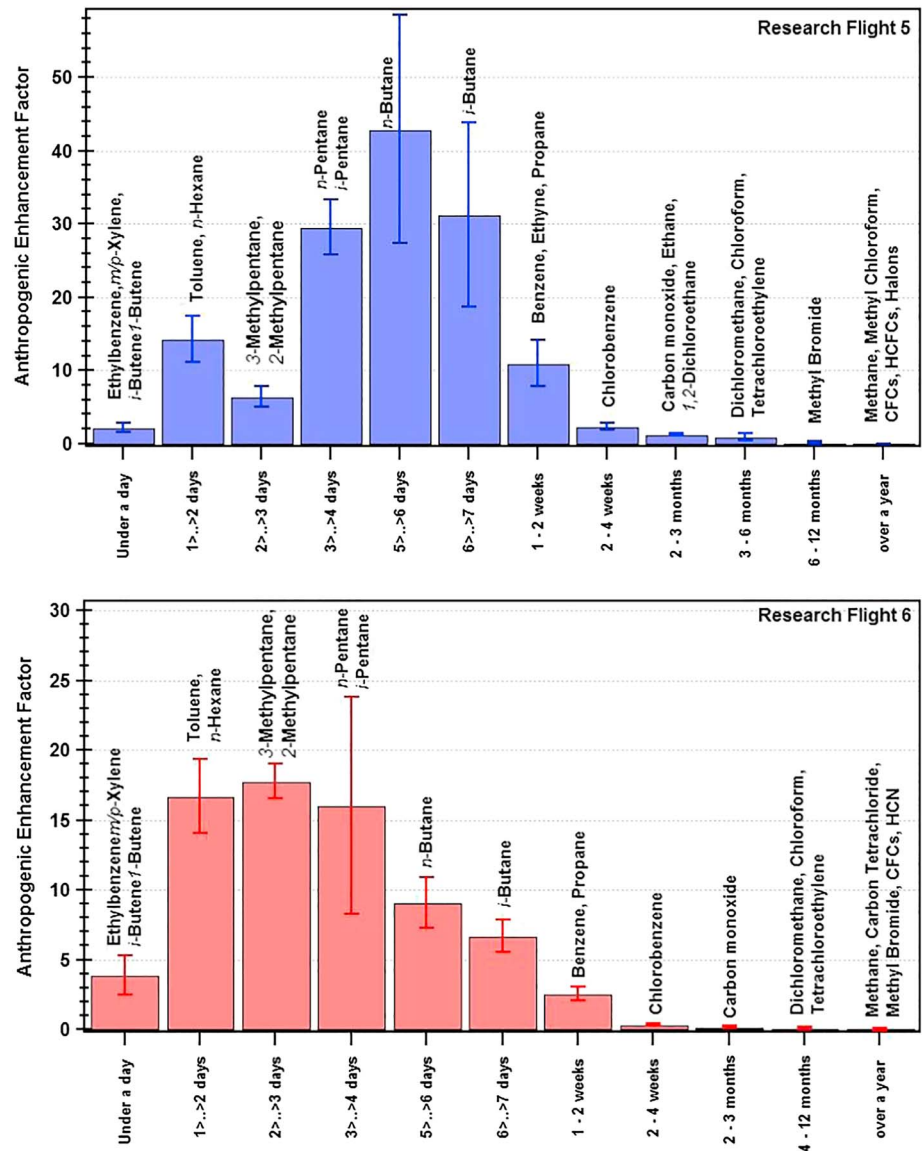


Figure 9. Anthropogenic Enhancement Factor (AEF, as defined in section 5.3) for flights RF05 (top) and RF06 (bottom) as a function of photochemical lifetimes of a selected subset of trace species.

photochemical lifetime of the gas in the atmosphere. This relationship seems to be critically dependent of the prescribed values for background, as choice of a background that results from just long photochemical decay does not produce the observed relationship. As has been shown from other studies of VOC ratios and photochemical ages (Johnston et al., 2002; McKeen & Liu, 1993; Parrish et al., 1992, 2007), loss of a trace gas in the atmosphere combines mixing with background air plus photochemical processing, and the low mixing ratio end-member (background) is typically some concentration higher than 0. Thus, the background concentration is controlled from a variety of mixing processes and photochemical loss.

The above result, showing agreement between photochemical age calculations, back trajectory analysis and AEF distribution peak demonstrates applicability of this theoretical concept to the real atmosphere, making it a potentially useful tool to assess impact of pollution plumes on the remote atmosphere.

5. Summary, Conclusions, and Broader Implications

Analysis of data collected during CONTRAST campaign provided the opportunity to study pathways of East Asian pollution transport into the deep tropics during boreal winter. During two flights of the CONTRAST

research campaign (RF05 and RF06) two consecutive shear line passages were observed, which were marked by significant increases of mixing ratios of anthropogenic tracers in the lowermost altitudes of the measurement profiles taken north of the advancing shear line.

Profile measurement taken on the north side of the stalled shear line (17°N, 138°E) during RF06 featured very sharp gradients in trace gas mixing ratios across the shear line boundary with enhancements confined to the lowermost troposphere (~2,000 m or >800 hPa). The most pronounced gradients were in mixing ratios of NMHCs, OVOCs, and a number of short-lived chlorinated solvents, all of which are identified as signatures of urban and industrial pollution. Backward trajectories calculated for this flight indicate that the emissions that contributed to the enhanced mixing ratios are most likely from industrialized areas of continental East Asia and northern Japan (~3-day transit time) and northeast Asia (>4.0-day transit time), and also possibly including emissions over central Siberia toward Europe (>10 days). The photochemical age of the intercepted air mass calculated using two different HC pairs was estimated to be on the order of 4.8 ± 1.6 days, in reasonable agreement with the back trajectory model.

Chemical tracer measurements taken during RF05 also saw marked enhancements of the mixing ratios of reactive trace gases in the lowermost part of the profile taken on the north side of the deteriorating front (<700 hPa), albeit mixing ratios measured were significantly lower compared to RF06. We attribute this to the fact that two shear line passages represent two different stages of the shear line evolution and overall strength of the front. Back trajectory analysis and photochemical age calculations indicate longer transport time from both the dynamical (~7 days until continental encounter) and chemical (photochemical day equivalent of 7.0 ± 1.8 days) data sets. Back trajectories in the case of RF05 similarly suggested influences from urbanized areas of continental East and northeast Asia (North and South Korea, E-NE China, and Mongolia) and Japan. Additionally, use of TERRA MOPITT instrument TIR/NIR January surface layer CO mixing ratios confirmed the hypothesis of mixing with anthropogenically influenced air based on the surface CO mixing ratios in the region well in excess of 150ppbv.

To quantify the contribution of transported anthropogenic tracers associated with migrating shear lines, we have defined an index, AEF, which represents the fractional change of a chemical species following each shear-line passage. This index shows a strong relationship with reactive trace gases photochemical lifetime and appears to have a unimodal distribution, which maximizes around the estimated photochemical lifetimes comparable to the transport duration as established using dynamical and chemical approaches. This relationship provides a useful diagnostic tool in studying atmospheric transport processes and should be examined in future studies.

These results document a mechanism of transport of anthropogenic pollution from midlatitudes of East Asia into the tropics during Northern Hemisphere winter. Together with previously published work (Ashfold et al., 2015; Lelieveld et al., 2001; Martin et al., 2002; Pochanart et al., 2004), we show influences of pollution originating over South and South-East Asia on both the Indian Ocean and the North Pacific. This implies a large spatial influence of the emissions originating over different parts of Asia on regional and global air quality. The mechanism discussed in this paper implies extensive (due to high frequency of shear line passages; Compo et al., 1999) transport of such pollution toward cleaner regions of Tropical Western Pacific, when extensive convective activity can deliver these pollutants directly into the TTL (Aschmann et al., 2009; Ashfold et al., 2012; Tissier & Legras, 2016; Pan et al., 2017).

Acknowledgments

We acknowledge the contributions of the pilots, engineers, and staff of the NCAR RAF for this project and all of the CONTRAST participants. The authors gratefully acknowledge the support of National Science Foundation (NSF) in funding this research under grant AGS1261657, as well as NCAR visitor program. The National Center for Atmospheric Research is sponsored by the National Science Foundation. CONTRAST data used in this study can be obtained from the CONTRAST Data Archive at EOL http://data.eol.ucar.edu/master_list/?project=CONTRAST. The MOPITT Version 7, Level 3 data are publicly available via <https://search.earthdata.nasa.gov/search?q=MOPITT&ok=MOPITT> (registration required).

References

- Akimoto, H., Mukai, H., Nishikawa, M., Murano, K., Hatakeyama, S., Liu, C.-M., et al. (1996). Long-range transport of ozone in the East Asian Pacific rim region. *Journal of Geophysical Research*, *101*, 1999–2010. <https://doi.org/10.1029/95jd00025>
- Andrews, S. J., Carpenter, L. J., Apel, E. C., Atlas, E., Donets, V., Hopkins, J. R., et al. (2016). A comparison of very short-lived halocarbon (VSLs) and DMS aircraft measurements in the tropical west Pacific from CAST, ATTREX and CONTRAST. *Atmospheric Measurement Techniques*, *9*(10), 5213–5225. <https://doi.org/10.5194/amt-9-5213-2016>
- Apel, E. C., Emmons, L. K., Karl, T., Flocke, F., Hills, A. J., Madronich, S., et al. (2010). Chemical evolution of volatile organic compounds in the outflow of the Mexico City Metropolitan area. *Atmospheric Chemistry and Physics*, *10*(5), 2353–2375. <https://doi.org/10.5194/acp-10-2353-2010>
- Apel, E. C., Hornbrook, R. S., Hills, A. J., Blake, N. J., Barth, M. C., Weinheimer, A., et al. (2015). Upper tropospheric ozone production from lightning NO_x-impacted convection: Smoke ingestion case study from the DC3 campaign. *Journal of Geophysical Research: Atmospheres*, *120*, 2505–2523. <https://doi.org/10.1002/2014JD022121>

- Apel, E. C., Olson, J. R., Crawford, J. H., Hornbrook, R. S., Hills, A. J., Cantrell, C. A., et al. (2012). Impact of the deep convection of isoprene and other reactive trace species on radicals and ozone in the upper troposphere. *Atmospheric Chemistry and Physics*, 12(2), 1135–1150. <https://doi.org/10.5194/acp-12-1135-2012>
- Aschmann, J., Sinnhuber, B., Atlas, E., & Schauffler, S. (2009). Modeling the transport of very short-lived substances into the tropical upper troposphere and lower stratosphere. *Atmospheric Chemistry and Physics Discussions*, 9(5), 18,511–18,543. <https://doi.org/10.5194/acpd-9-18511-2009>
- Ashfold, M., Harris, N., Atlas, E., Manning, A., & Pyle, J. (2012). Transport of short-lived species into the Tropical Tropopause Layer. *Atmospheric Chemistry and Physics Discussions*, 12(1), 441–478. <https://doi.org/10.5194/acpd-12-441-2012>
- Ashfold, M. J., Pyle, J. A., Robinson, A. D., Meneguz, E., Nadzir, M. S. M., Phang, S. M., et al. (2015). Rapid transport of East Asian pollution to the deep tropics. *Atmospheric Chemistry and Physics*, 15(6), 3565–3573. <https://doi.org/10.5194/acp-15-3565-2015>
- Atkinson, R. (2003). Kinetics of the gas-phase reactions of OH radicals with alkanes and cycloalkanes. *Atmospheric Chemistry and Physics*, 3(6), 2233–2307. <https://doi.org/10.5194/acp-3-2233-2003>
- Atkinson, R. (2007). Gas-phase tropospheric chemistry of organic compounds: A review. *Atmospheric Environment*, 41, 200–240. <https://doi.org/10.1016/j.atmosenv.2007.10.068>
- Avery, M. A., Westberg, D. J., Fuelberg, H. E., Newell, R. E., Anderson, B. E., Vay, S. A., et al. (2001). Chemical transport across the ITCZ in the Central Pacific during an El Niño–Southern Oscillation cold phase event in March–April 1999. *Journal of Geophysical Research*, 106(D23), 32539–32553. <https://doi.org/10.1029/2001jd000728>
- Barletta, B., Meinardi, S., Sherwood Rowland, F., Chan, C.-Y., Wang, X., Zou, S., et al. (2005). Volatile organic compounds in 43 Chinese cities. *Atmospheric Environment*, 39(32), 5979–5990. <https://doi.org/10.1016/j.atmosenv.2005.06.029>
- Barletta, B., Meinardi, S., Simpson, I. J., Atlas, E. L., Beyersdorf, A. J., Baker, A. K., et al. (2009). Characterization of volatile organic compounds (VOCs) in Asian and north American pollution plumes during INTEX-B: Identification of specific Chinese air mass tracers. *Atmospheric Chemistry and Physics*, 9(14), 5371–5388. <https://doi.org/10.5194/acp-9-5371-2009>
- Blake, D. R., Chen, T.-Y., Smith, T. W., Wang, C. J. L., Wingenter, O. W., Blake, N. J., et al. (1996). Three-dimensional distribution of non-methane hydrocarbons and halocarbons over the northwestern Pacific during the 1991 Pacific Exploratory Mission (PEM-West A). *Journal of Geophysical Research*, 101(D1), 1763–1778. <https://doi.org/10.1029/95jd02707>
- Blake, N. J., Blake, D. R., Simpson, I. J., Meinardi, S., Swanson, A. L., Lopez, J. P., et al. (2003). NMHCs and halocarbons in Asian continental outflow during the Transport and Chemical Evolution over the Pacific (TRACE-P) Field Campaign: Comparison With PEM-West B. *Journal of Geophysical Research*, 108(D20), 8806. <https://doi.org/10.1029/2002JD003367>
- Blake, N. J., Blake, D. R., Simpson, I. J., Lopez, J. P., Johnston, N. A. C., Swanson, A. L., et al. (2001). Large-scale latitudinal and vertical distributions of NMHCs and selected halocarbons in the troposphere over the Pacific Ocean during the March–April 1999 Pacific Exploratory Mission (PEM-Tropics B). *Journal of Geophysical Research*, 106(D23), 32,627–32,644. <https://doi.org/10.1029/2000jd900773>
- Bo, Y., Cai, H., & Xie, S. D. (2008). Spatial and temporal variation of historical anthropogenic NMVOCs emission inventories in China. *Atmospheric Chemistry and Physics*, 8(23), 7297–7316. <https://doi.org/10.5194/acp-8-7297-2008>
- Bowman, K. P. (1993). Large-scale isentropic mixing properties of the Antarctic polar vortex from analyzed winds. *Journal of Geophysical Research*, 98(D12), 23,013–23,027. <https://doi.org/10.1029/93JD02599>
- Bowman, K. P., & Carrie, G. D. (2002). The mean-meridional transport circulation of the troposphere in an idealized GCM. *Journal of the Atmospheric Sciences*, 59(9), 1502–1514. [https://doi.org/10.1175/1520-0469\(2002\)059<1502:tmmtco>2.0.co;2](https://doi.org/10.1175/1520-0469(2002)059<1502:tmmtco>2.0.co;2)
- Burkholder, J. B., Sander, S. P., Abbatt, J., Barker, J., Huie, R., Kolb, C. E., et al. (2015). Chemical Kinetics and Photochemical Data for Use in Atmospheric Studies, Evaluation Number 18. 10.13140/RG.2.1.2504.2806
- Byeon, S. H., Lee, J. G., & Kim, J. K. (2010). Patterns of the main VOCs concentration in ambient air around Shiwha Area. *J. Kor. Soc. Environ. Eng.*, 32(1), 1229–1236.
- Carpenter, L. J., Reimann, S., Burkholder, J. B., Clerbaux, C., Hall, B., Hossaini, R., et al. (2014). Chapter 1: Update on ozone-depleting substances (ODSs) and other gases of interest to the Montreal protocol. In C. A. Ennis (Ed.), *Scientific assessment of ozone depletion: 2014. (Global ozone research and monitoring project report; no. 55)* (pp. 31–50). Geneva: World Meteorological Organization (WMO).
- Compo, G. P., Kiladis, G. N., & Webster, P. J. (1999). The horizontal and vertical structure of east Asian winter monsoon pressure surges. *Quarterly Journal of the Royal Meteorological Society*, 125(553), 29–54. <https://doi.org/10.1002/qj.4971255304>
- Cooper, O. R., Parrish, D. D., Stohl, A., Trainer, M., Nedelec, P., Thouret, V., et al. (2010). Increasing springtime ozone mixing ratios in the free troposphere over western North America. *Nature*, 463(7279), 344–348. <https://doi.org/10.1038/nature08708>
- Deeter, M. N., Edwards, D. P., Francis, G. L., Gille, J. C., Martínez-Alonso, S., Worden, H. M., & Sweeney, C. (2017). A climate-scale satellite record for carbon monoxide: The MOPITT version 7 product. *Atmospheric Measurement Techniques*, 10(7), 2533–2555. <https://doi.org/10.5194/amt-10-2533-2017>
- Flocke, F., Herman, R. L., Salawitch, R. J., Atlas, E., Webster, C. R., Schauffler, S. M., et al. (1999). An examination of chemistry and transport processes in the tropical lower stratosphere using observations of long-lived and short-lived compounds obtained during STRAT and POLARIS. *Journal of Geophysical Research*, 104(D21), 26,625–26,642. <https://doi.org/10.1029/1999JD900504>
- Gao, J., Zhang, J., Li, H., Li, L., Xu, L., Zhang, Y., et al. (2018). Comparative study of volatile organic compounds in ambient air using observed mixing ratios and initial mixing ratios taking chemical loss into account—A case study in a typical urban area in Beijing. *Science of the Total Environment*, 628–629, 791–804. <https://doi.org/10.1016/j.scitotenv.2018.01.175>
- Gerbig, C., Schmitgen, S., Kley, D., Volz-Thomas, A., Dewey, K., & Haaks, D. (1999). An improved fastresponse vacuum-UV resonance fluorescence CO instrument. *Journal of Geophysical Research*, 104(D1), 1699–1704. <https://doi.org/10.1029/1998JD100031>
- Gregory, G., Fuelberg, H., Longmore, S., Anderson, B., Collins, J., & Blake, D. (1996). Chemical characteristics of tropospheric air over the tropical South Atlantic Ocean: Relationship to trajectory history. *Journal Of Geophysical Research*, 101(D19), 23,957–23,972. <https://doi.org/10.1029/96JD01160>
- Helmig, D., Hueber, J., Tans, P. (2017) Non-methane hydrocarbons from the NOAA ESRL surface network, 2004–2016. [online] Available at: http://ftp://aftp.cmdl.noaa.gov/data/trace_gases/voc/ [Accessed 8 Dec. 2017].
- Hilboll, A., Richter, A., & Burrows, J. P. (2013). Long-term changes of tropospheric NO₂ over megacities derived from multiple satellite instruments. *Atmospheric Chemistry and Physics*, 13(8), 4145–4169. <https://doi.org/10.5194/acp-13-4145-2013>
- Hoell, J. M., Davis, D. D., Liu, S. C., Newell, R., Shipham, M., Akimoto, H., et al. (1996). Pacific Exploratory Mission–West A (PEM–West A): September–October 1991. *Journal of Geophysical Research*, 101(D1), 1641–1653. <https://doi.org/10.1029/95JD00622>
- Jacob, D. J., Logan, J. A., & Murti, P. P. (1999). Effect of rising Asian emissions on surface ozone in the United States. *Geophysical Research Letters*, 26(14), 2175–2178. <https://doi.org/10.1029/1999GL900450>
- Jaffe, D., Anderson, T., Covert, D., Kotchenruther, R., Trost, B., Danielson, J., et al. (1999). Transport of Asian air pollution to North America. *Geophysical Research Letters*, 26(6), 711–714. <https://doi.org/10.1029/1999GL900100>

- Jaffe, D., McKendry, I., Anderson, T., & Price, H. (2003). Six 'new' episodes of trans-Pacific transport of air pollutants. *Atmospheric Environment*, 37(3), 391–404. [https://doi.org/10.1016/S13522310\(02\)00862-2](https://doi.org/10.1016/S13522310(02)00862-2)
- Jaffe, D., Price, H., Parrish, D., Goldstein, A., & Harris, J. (2003). Increasing background ozone during spring on the west coast of North America. *Geophysical Research Letters*, 30(12), 1613. <https://doi.org/10.1029/2003GL017024>
- Jia, C., Mao, X., Huang, T., Liang, X., Wang, Y., Shen, Y., et al. (2016). Non-methane hydrocarbons (NMHCs) and their contribution to ozone formation potential in a petrochemical industrialized city, Northwest China. *Atmospheric Research*, 169, 225–236. <https://doi.org/10.1016/j.atmosres.2015.10.006>
- Johnston, N. A. C., Colman, J. J., Blake, D. R., Prather, M. J., & Rowland, F. S. (2002). On the variability of tropospheric gases: Sampling, loss patterns, and lifetime. *Journal of Geophysical Research*, 107(D11), 4111. <https://doi.org/10.1029/2001jd000669>
- Kim, K., Shon, Z., Kim, M., Sunwoo, Y., Jeon, E., & Hong, J. (2008). Major aromatic VOC in the ambient air in the proximity of an urban landfill facility. *Journal of Hazardous Materials*, 150(3), 754–764. <https://doi.org/10.1016/j.jhazmat.2007.05.038>
- Kurokawa, J., Ohara, T., Morikawa, T., Hanayama, S., Janssens-Maenhout, G., Fukui, T., et al. (2013). Emissions of air pollutants and greenhouse gases over Asian regions during 2000–2008: Regional emission inventory in ASia (REAS) version 2. *Atmospheric Chemistry and Physics*, 13(21), 11,019–11,058. <https://doi.org/10.5194/acp-13-11019-2013>
- Lam, K. S., Wang, T. J., Wu, C. L., & Li, Y. S. (2005). Study on an ozone episode in hot season in Hong Kong and transboundary air pollution over Pearl River Delta region of China. *Atmospheric Environment*, 39(11), 1967–1977. <https://doi.org/10.1016/j.atmosenv.2004.11.023>
- Lawrence, M. G., & Lelieveld, J. (2010). Atmospheric pollutant outflow from southern Asia: A review. *Atmospheric Chemistry and Physics*, 10(22), 11,017–11,096. <https://doi.org/10.5194/acp-10-11017-2010>
- Lee, C., Kim, Y. J., Hong, S., Lee, H., Jung, J., Choi, Y., et al. (2005). Measurement of atmospheric formaldehyde and monoaromatic hydrocarbons using differential optical absorption spectroscopy during winter and summer intensive periods in Seoul, Korea. *Water, Air, and Soil Pollution*, 166(1–4), 181–195. <https://doi.org/10.1007/s11270-005-7308-6>
- Lelieveld, J., Crutzen, P. J., Ramanathan, V., Andreae, M. O., Brenninkmeijer, C. A. M., Campos, T., et al. (2001). The Indian Ocean Experiment: Widespread Air Pollution from South and Southeast Asia. *Science*, 291(5506), 1031–1036.
- Li, J., Xie, S. D., Zeng, L. M., Li, L. Y., Li, Y. Q., & Wu, R. R. (2015). Characterization of ambient volatile organic compounds and their sources in Beijing, before, during, and after Asia-Pacific Economic Cooperation China 2014. *Atmospheric Chemistry and Physics*, 15(14), 7945–7959. <https://doi.org/10.5194/acp-15-7945-2015>
- Li, L., Chen, Y., Zeng, L., Shao, M., Xie, S., Chen, W., et al. (2014). Biomass burning contribution to ambient volatile organic compounds (VOCs) in the Chengdu–Chongqing Region (CCR), China. *Atmospheric Environment*, 99, 403–410. <https://doi.org/10.1016/j.atmosenv.2014.09.067>
- Lin, J. T. (2012). Satellite constraint for emissions of nitrogen oxides from anthropogenic, lightning and soil sources over East China on a high-resolution grid. *Atmospheric Chemistry and Physics*, 12(6), 2881–2898. <https://doi.org/10.5194/acp-12-2881-2012>
- Lin, M., Fiore, A. M., Cooper, O. R., Horowitz, L. W., Langford, A. O., Levy, H., et al. (2012). Springtime high surface ozone events over the western United States: Quantifying the role of stratospheric intrusions. *Journal of Geophysical Research*, 117, D00V22. <https://doi.org/10.1029/2012jd018151>
- Lin, M., Fiore, A. M., Horowitz, L. W., Cooper, O. R., Naik, V., Holloway, J., et al. (2012). Transport of Asian ozone pollution into surface air over the western United States in spring. *Journal of Geophysical Research*, 117, D00V07. <https://doi.org/10.1029/2011jd016961>
- Martin, B. D., Fuelberg, H. E., Blake, N. J., Crawford, J. H., Logan, J. A., Blake, D. R., & Sachse, G. W. (2002). Long-range transport of Asian outflow to the equatorial Pacific. *Journal of Geophysical Research*, 108(D2), 8233. <https://doi.org/10.1029/2001jd001418>
- McCulloch, A., Aucott, M. L., Benkovitz, C. M., Graedel, T. E., Kleiman, G., Midgley, P. M., & Li, Y.-F. (1999). Global emissions of hydrogen chloride and chloromethane from coal combustion, incineration and industrial activities: Reactive Chlorine Emissions Inventory. *Journal of Geophysical Research*, 104(D7), 8391–8403. <https://doi.org/10.1029/1999JD900025>
- McKeen, S. A., & Liu, S. C. (1993). Hydrocarbon ratios and photochemical history of air masses. *Geophysical Research Letters*, 20(21), 2363–2366. <https://doi.org/10.1029/93GL02527>
- McKeen, S. A., Liu, S. C., Hsie, E. Y., Lin, X., Bradshaw, J. D., Smyth, S., et al. (1996). Hydrocarbon ratios during PEM-WEST A: A model perspective. *Journal of Geophysical Research*, 101(D1), 2087–2109. <https://doi.org/10.1029/95jd02733>
- Morino, Y., Ohara, T., Yokouchi, Y., & Ooki, A. (2011). Comprehensive source apportionment of volatile organic compounds using observational data, two receptor models, and an emission inventory in Tokyo metropolitan area. *Journal of Geophysical Research*, 116, D02311. <https://doi.org/10.1029/2010jd014762>
- Na, K., Kim, Y. P., & Moon, K. C. (2002). Seasonal variation of the C2–C9 hydrocarbons concentrations and compositions emitted from motor vehicles in a Seoul tunnel. *Atmospheric Environment*, 36(12), 1969–1978. [https://doi.org/10.1016/S1352-2310\(02\)00149-8](https://doi.org/10.1016/S1352-2310(02)00149-8)
- Ohura, T., Amagai, T., Senga, Y., & Fusaya, M. (2006). Organic air pollutants inside and outside residences in Shimizu, Japan: Levels, sources and risks. *Science of the Total Environment*, 366(2–3), 485–499. <https://doi.org/10.1016/j.scitotenv.2005.10.005>
- Pan, L. L., Atlas, E. L., Salawitch, R. J., Honomichl, S. B., Bresch, J. F., Randel, W. J., et al. (2017). The Convective Transport of Active Species in the Tropics (CONTRAST) experiment. *Bulletin of the American Meteorological Society*, 98(1), 106–128. <https://doi.org/10.1175/bams-d-1400272.1>
- Pan, L. L., Honomichl, S. B., Randel, W. J., Apel, E. C., Atlas, E. L., Beaton, S. P., et al. (2015). Bimodal distribution of free tropospheric ozone over the tropical western Pacific revealed by airborne observations. *Geophysical Research Letters*, 42, 7844–7851. <https://doi.org/10.1002/2015GL065562>
- Parrish, D. D., Hahn, C. J., Williams, E. J., Norton, R. B., Fehsenfeld, F. C., Singh, H. B., et al. (1992). Indications of photochemical histories of Pacific air masses from measurements of atmospheric trace species at Point Arena, California. *Journal of Geophysical Research*, 97(D14), 15,883–15,901. <https://doi.org/10.1029/92JD01242>
- Parrish, D. D., Stohl, A., Forster, C., Atlas, E. L., Blake, D. R., Goldan, P. D., et al. (2007). Effects of mixing on evolution of hydrocarbon ratios in the troposphere. *Journal of Geophysical Research*, 112, D10S34. <https://doi.org/10.1029/2006jd007583>
- Patra, P. K., Krol, M. C., Montzka, S. A., Arnold, T., Atlas, E. L., Lintner, B. R., et al. (2014). Observational evidence for interhemispheric hydroxyl-radical parity. *Nature*, 513(7517), 219–223. <https://doi.org/10.1038/nature13721>
- Perry, R. A., Atkinson, R., & Pitts, J. N. (1977). Kinetics and mechanism of the gas phase reaction of hydroxyl radicals with aromatic hydrocarbons over the temperature range 296–473 K. *The Journal of Physical Chemistry*, 81(4), 296–304. <https://doi.org/10.1021/j100519a004>
- Phadnis, M. J. (2002). On the evolution of pollution from South and Southeast Asia during the winterspring monsoon. *Journal of Geophysical Research*, 107(D24), 4790. <https://doi.org/10.1029/2002jd002190>
- Pochanart, P., Wild, O., & Akimoto, H. (2004). Air pollution import to and export from East Asia. In A. Stohl (Ed.), *Air pollution: Intercontinental transport of air pollution* (pp. 99–130). Berlin, Heidelberg: Springer Berlin Heidelberg.
- Price, H. U., Jaffe, D. A., Doskey, P. V., McKendry, I., & Anderson, T. L. (2003). Vertical profiles of O₃, aerosols, CO and NMHCs in the Northeast Pacific during the TRACE-P and ACE-ASIA experiments. *Journal of Geophysical Research*, 108(D20), 8799. <https://doi.org/10.1029/2002JD002930>

- Prinn, R. G., Weiss, R. F., Fraser, P. J., Simmonds, P. G., Cunnold, D. M., Alyea, F. N., et al. (2000). A history of chemically and radiatively important gases in air deduced from ALE/GAGE/AGAGE. *Journal of Geophysical Research*, *105*(D14), 17,751–17,792. <https://doi.org/10.1029/2000jd900141>
- Richter, A., Burrows, J. P., Nusz, H., Granier, C., & Niemeier, U. (2005). Increase in tropospheric nitrogen dioxide over China observed from space. *Nature*, *437*(7055), 129–132. <https://doi.org/10.1038/nature04092>
- Roberts, J. M., Fehsenfeld, F. C., Liu, S. C., Bollinger, M. J., Hahn, C., Albritton, D. L., & Sievers, R. E. (1984). Measurements of aromatic hydrocarbon ratios and NO_x concentrations in the rural troposphere: Observation of air mass photochemical aging and NO_x removal. *Atmospheric Environment (1967)*, *18*(11), 2421–2432. [https://doi.org/10.1016/0004-6981\(84\)90012-X](https://doi.org/10.1016/0004-6981(84)90012-X)
- Schauffler, S. M., Atlas, E. L., Blake, D. R., Flocke, F., Lueb, R. A., Lee-Taylor, J. M., et al. (1999). Distributions of brominated organic compounds in the troposphere and lower stratosphere. *Journal of Geophysical Research*, *104*(D17), 21,513–21,535. <https://doi.org/10.1029/1999JD900197>
- Shetter, R. E., & Müller, M. (1999). Photolysis frequency measurements using actinic flux spectroradiometry during the PEM-Tropics mission: Instrumentation description and some results. *Journal of Geophysical Research*, *104*(D5), 5647–5661. <https://doi.org/10.1029/98JD01381>
- Skamarock, W. C., Klemp, J. B., Dudhia, J., Gill, D. O., Barker, D. M., Duda, M. G., et al. (2008). A description of the Advanced Research WRF version 3, NCAR Tech. Note NCAR/TN-475+STR (113 pp.)
- Tanimoto, H., Ohara, T., & Uno, I. (2009). Asian anthropogenic emissions and decadal trends in springtime tropospheric ozone over Japan: 1998–2007. *Geophysical Research Letters*, *36*, L23802. <https://doi.org/10.1029/2009GL041382>
- Tanimoto, H., Sawa, Y., Yonemura, S., Yumimoto, K., Matsueda, H., Uno, I., et al. (2008). Diagnosing recent CO emissions and ozone evolution in East Asia using coordinated surface observations, adjoint inverse modeling, and MOPITT satellite data. *Atmospheric Chemistry and Physics*, *8*(14), 3867–3880. <https://doi.org/10.5194/acp-8-3867-2008>
- Tissier, A., & Legras, B. (2016). Convective sources of trajectories traversing the tropical tropopause layer. *Atmospheric Chemistry and Physics*, *16*(5), 3383–3398. <https://doi.org/10.5194/acp-16-3383-2016>
- Uchiyama, S., Tomizawa, T., Tokoro, A., Aoki, M., Hishiki, M., Yamada, T., et al. (2015). Gaseous chemical compounds in indoor and outdoor air of 602 houses throughout Japan in winter and summer. *Environmental Research*, *137*, 364–372. <https://doi.org/10.1016/j.envres.2014.12.005>
- Wang, G., Cheng, S., Wei, W., Zhou, Y., Yao, S., & Zhang, H. (2016). Characteristics and source apportionment of VOCs in the suburban area of Beijing, China. *Atmospheric Pollution Research*, *7*(4), 711–724. <https://doi.org/10.1016/j.apr.2016.03.006>
- Wang, Y., Wang, M., Zhang, R., Ghan, S. J., Lin, Y., Hu, J., et al. (2014). Assessing the effects of anthropogenic aerosols on Pacific storm track using a multiscale global climate model. *Proceedings of the National Academy of Sciences of the USA*, *111*(19), 6894–6899. <https://doi.org/10.1073/pnas.1403364111>
- Wang, L., Wu, R., & Xu, C. (2013). Atmospheric oxidation mechanism of benzene. Fates of alkoxy radical intermediates and revised mechanism. *The Journal of Physical Chemistry A*, *117*(51), 14,163–14,168. <https://doi.org/10.1021/jp4101762>
- Wild, O., & Akimoto, H. (2001). Intercontinental transport of ozone and its precursors in a three-dimensional global CTM. *Journal of Geophysical Research*, *106*(D21), 27,729–27,744. <https://doi.org/10.1029/2000jd000123>
- Wu, R., Pan, S., Li, Y., & Wang, L. (2014). Atmospheric oxidation mechanism of toluene. *The Journal of Physical Chemistry A*, *118*(25), 4533–4547. <https://doi.org/10.1021/jp500077f>
- Zhang, H., Li, H., Zhang, Q., Zhang, Y., Zhang, W., Wang, X., et al. (2017). Atmospheric volatile organic compounds in a typical urban area of Beijing: Pollution characterization, health risk assessment and source apportionment. *Atmosphere*, *8*(12), 61. <https://doi.org/10.3390/atmos8030061>
- Zhang, Y., Mu, Y., Liu, J., & Mellouki, A. (2012). Levels, sources and health risks of carbonyls and BTEX in the ambient air of Beijing, China. *Journal of Environmental Sciences*, *24*(1), 124–130. [https://doi.org/10.1016/s1001-0742\(11\)60735-3](https://doi.org/10.1016/s1001-0742(11)60735-3)